Advanced NanoBiomed Research

ADVANCED NANOBIOMED RESEARCH Open Access

www.advnanobiomedres.com

RESEARCH ARTICLE OPEN ACCESS

NUAK2 Inhibition Enhances Macromolecular Drug Delivery in a 3D Fibrotic Model of the Pancreatic Tumor Microenvironment

Misaki Nakamura[1] | Hiroyoshi Y. Tanaka[1] | Mayu Ohira[1] | Haruko Ohta-Okano[1] | Reika Nakamura[1] | Yu Seno[1] | Saaya Yara[1] | Sakura Fujita[1] | Daichi Shibata[1] | Masaya Yamamoto[2,3] | Shinichi Toyooka[4] | Kensuke Osada[5] | Horacio Cabral[6] | Atsushi Masamune[7] | Mitsunobu R. Kano[8]

[1]Department of Pharmaceutical Biomedicine, Graduate School of Medicine, Dentistry and Pharmaceutical Sciences, Okayama University, Okayama-Shi, Japan | [2]Department of Materials Processing, Graduate School of Engineering, Tohoku University, Sendai-Shi, Japan | [3]Division of Biomedical Engineering for Diagnosis and Treatment, Graduate School of Biomedical Engineering, Tohoku University, Sendai-Shi, Japan | [4]Department of General Thoracic Surgery and Breast and Endocrinological Surgery, Graduate School of Medicine, Dentistry and Pharmaceutical Sciences, Okayama University, Okayama-Shi, Japan | [5]Department of Molecular Imaging and Theranostics, Institute for Quantum Medical Science, National Institutes for Quantum Sciences and Technology (QST), Chiba-Shi, Japan | [6]Department of Bioengineering, Graduate School of Engineering, The University of Tokyo, Tokyo, Japan | [7]Division of Gastroenterology, Graduate School of Medicine, Tohoku University, Sendai-Shi, Japan | [8]Department of Pharmaceutical Biomedicine, Graduate School of Interdisciplinary Science and Engineering in Health Systems, Okayama University, Okayama-Shi, Japan

Correspondence: Hiroyoshi Y. Tanaka (hiroyoshi.y.tanaka@okayama-u.ac.jp) | Mitsunobu R. Kano (mikano-tky@umin.net)

Received: 17 September 2025 | **Revised:** 19 December 2025 | **Accepted:** 20 January 2026

Keywords: fibrosis | nanomedicine | NUAK kinase | pancreatic cancer | tumor microenvironment

ABSTRACT

Pancreatic ductal adenocarcinoma (PDAC) features a fibrotic tumor microenvironment that impedes drug delivery and significantly limits the successful clinical application of nanomedicines. Targeting signaling in pancreatic stellate cells (PSCs), which drive fibrosis via excessive secretion of extracellular matrix proteins such as collagen I, may be useful in overcoming this fibrotic barrier. The AMPK-related kinases NUAK1/2 have recently gained interest as promoters of fibrosis, but whether they play a profibrotic role in PSCs remains unknown. Here, patient PSCs are used to assess NUAK1/2 involvement in the PDAC fibrotic barrier. Leveraging a 3D cell culture model of PDAC fibrosis, the effect of targeting NUAK1/2 on the permeability of macromolecular dextrans of various sizes, as well as physiologically relevant macromolecules, albumin and IgG, and clinical nanomedicines, Doxil and Abraxane, is investigated. NUAK1/2 inhibition is shown to diminish collagen I to enhance macromolecular permeability, via a mechanism independent of established pathways involving transforming growth factor-β (TGFβ) and yes-associated protein (YAP). Through isoform-specific knockdown, predominant NUAK2 involvement is demonstrated. Mechanistically, actin stress fiber regulation by NUAK2 is shown to be important. Altogether, these results show in vitro that NUAK2 promotes fibrotic signaling in PSCs and may be targeted to enhance macromolecular drug delivery in PDAC.

Abbreviations: αSMA, α-smooth muscle actin; AMPK, AMP-activated protein kinase; DMSO, dimethyl sulfoxide; FITC, fluorescein isothiocyanate; MLCK, myosin light chain kinase; O/N, overnight; PBS, phosphate-buffered saline; PDAC, pancreatic ductal adenocarcinoma; PFA, paraformaldehyde; prPSC, primary pancreatic stellate cell; PSC, pancreatic stellate cell; ROCK, Rho-associated kinase; RT, room temperature; RT-qPCR, reverse transcription-quantitative polymerase chain reaction; SD, standard deviation; TGFβ, transforming growth factor-β; YAP, yes-associated protein.

Misaki Nakamura and Hiroyoshi Y. Tanaka contributed equally to this study.

1 | Introduction

Pancreatic ductal adenocarcinomas (PDAC), which account for around 95% of pancreatic cancers, feature a fibrotic tumor microenvironment characterized by excessive deposition of extracellular matrix proteins such as collagen I. Fibrosis is a significant barrier to drug delivery, thus contributing to the poor prognosis of PDAC patients, with a 5-year survival of approximately 10% [1]. The fibrotic barrier is especially problematic for the delivery of macromolecular drugs, such as albumin-based drug carriers, therapeutic IgG antibodies, and nanomedicines. Therapeutic strategies to overcome the fibrotic barrier are thus necessary for the successful clinical application of macromolecular drugs and to improve patient outcome in PDAC [2]. The failure of stromal ablation strategies that reduce fibrotic tissue argues for the need for approaches that modulate fibrotic signaling mechanisms to achieve a favorable stromal phenotype [3]. However, the molecular and cellular mechanisms underlying fibrotic barrier generation remain incompletely understood.

Pancreatic stellate cells (PSC), which are resident fibroblastic cells of the pancreas, drive the fibrotic process [4, 5]. Targeting fibrotic signaling in PSCs thus may be effective in overcoming the fibrotic barrier. Recently, NUAK1, a member of the AMP-activated protein kinase (AMPK)-related kinase family of serine/threonine kinases [6, 7], has gained interest for promoting renal, hepatic, and pulmonary fibrosis [8]. Interestingly, the transforming growth factor-β (TGFβ) and yes-associated protein (YAP) signaling pathways, both of which promote fibrotic barrier generation in PDAC [9, 10], have been reported to transcriptionally regulate NUAK1 and its closely related isoform NUAK2 [8, 11, 12]. In turn, NUAK1/2 kinases reciprocally modulate TGFβ and YAP signaling pathway outputs [11, 12]. NUAK1/2 kinases thus seem well-positioned to play an integral part in fibrotic signaling in PSCs, but this notion has not been previously tested and the involvement of NUAK1/2 in the PDAC fibrotic barrier remains unknown.

Here, we used PDAC patient-derived PSCs to investigate whether NUAK1/2 kinases participate in fibrotic signaling. To assess whether NUAK1/2 targeting enhances macromolecular permeability, we leveraged a 3D cell culture model of PDAC fibrosis that recapitulates the clinically observed, median thickness of fibrotic tissue that an intravenous drug must penetrate to reach tumor cells, 10–30 μm [9, 13, 14]. We assessed not only macromolecular dextrans of different sizes, but also physiologically and therapeutically relevant macromolecules, albumin and IgG, as well as clinical nanomedicines, Doxil and Abraxane. We show that pharmacological targeting of NUAK1/2 enhances macromolecular permeability by diminishing collagen I expression in PSCs. Through isoform-specific knockdowns, stronger contribution of NUAK2 over NUAK1 in regulating collagen I expression and macromolecular permeability is demonstrated. Surprisingly, NUAK1/2 kinases are shown to largely function independently of known pro-fibrotic TGFβ and YAP signaling pathways in PSCs. Mechanistically, we reveal the importance of actin stress fiber regulation by NUAK2. Altogether, we demonstrate in vitro that NUAK2 participates in fibrotic signaling in PSCs and may be targeted to enhance macromolecular drug delivery through the fibrotic barrier in PDAC.

2 | Results

2.1 | Pharmacological Inhibition of NUAK1/2 Kinases Enhances Macromolecular Permeability of 3D-PDAC Fibrotic Tissues

To assess whether NUAK1/2 is involved in the PDAC fibrotic barrier, we utilized a 3D cell culture model of PDAC fibrosis (3D-PDAC fibrotic tissues), constructed by the cell accumulation technique using PSCs derived from patients with PDAC [13]. Immortalized PSCs were mainly used due to faster proliferation compared to primary PSCs (prPSCs) and the requirement for large cell numbers in constructing the 3D tissues. PrPSCs were, however, also used to confirm key results. The 3D-PDAC fibrotic tissue model recapitulates the median thickness of fibrotic tissue observed in clinical PDAC specimens [13, 14], and its use enables rapid and reproducible correlation of the effect of perturbing particular signaling pathways on PSC phenotype with the effect on macromolecular permeability of fibrotic tissues [9, 15]. The 3D-PDAC fibrotic tissue model is thus useful for identifying potential targets to overcome the fibrotic barrier.

While the NUAK1/2 inhibitor WZ4003 [16] at 10 μM decreased the growth of PSCs cultured in 2D on conventional plastic by ~50% (Figure 1A–D), neither 3D-PDAC fibrotic tissue thickness nor cell viability was significantly reduced by any of the concentrations tested (Figure 1E–J). The relatively higher viability of PSCs in 3D PDAC-fibrotic tissues against inhibitor treatment compared to 3D culture is in line with our previous reports [9, 15], likely resulting from altered microenvironmental cues within the 3D experimental setup [17]. Importantly, 10 μM WZ4003 enhanced the permeability of 3D-PDAC fibrotic tissues to fluorescein isothiocyanate (FITC)-labeled dextrans with average molecular weights of 70 kDa (Figure 1K,L), 150 kDa (Figure 1M,N), or 2000 kDa (Figure 1O,P). Permeation of physiological macromolecules, albumin (Figure 1Q,R) and IgG (Figure 1S,T), was also enhanced. These results altogether suggest that NUAK1/2 inhibition enhances macromolecular permeability of 3D-PDAC fibrotic tissues. Consistent with the results obtained with immortalized PSCs, 10 μM WZ4003 also enhanced permeability of 3D-PDAC fibrotic tissues constructed using prPSCs from two patients with PDAC (Figure S1A–J). Because WZ4003 did not significantly decrease 3D-PDAC fibrotic tissue thickness or viability, its effect does not appear to be exerted by reduction of stromal tissue content altogether (i.e., stromal ablation).

Enhanced permeability to albumin and IgG by WZ4003 treatment has broad therapeutic implications given their widespread use as carriers and for active targeting, respectively [18]. To further investigate this aspect, we tested whether the increase in macromolecular permeability by WZ4003 enhances the therapeutic effect of two clinical nanomedicines, Doxil (liposomal doxorubicin) and Abraxane (nab-paclitaxel). Doxil or Abraxane was loaded onto 3D-PDAC fibrotic tissues pretreated with WZ4003; then, the media beneath the culture inserts containing the permeated nanomedicines were collected and used to treat the PDAC cell-line MiaPaCa-2 to compare the effect on cell growth (Figure 1U). As expected, the interposition of 3D-PDAC fibrotic tissues acted as a fibrotic barrier and attenuated the therapeutic effects of Doxil and Abraxane compared to direct administration of these nanomedicines to MiaPaCa-2

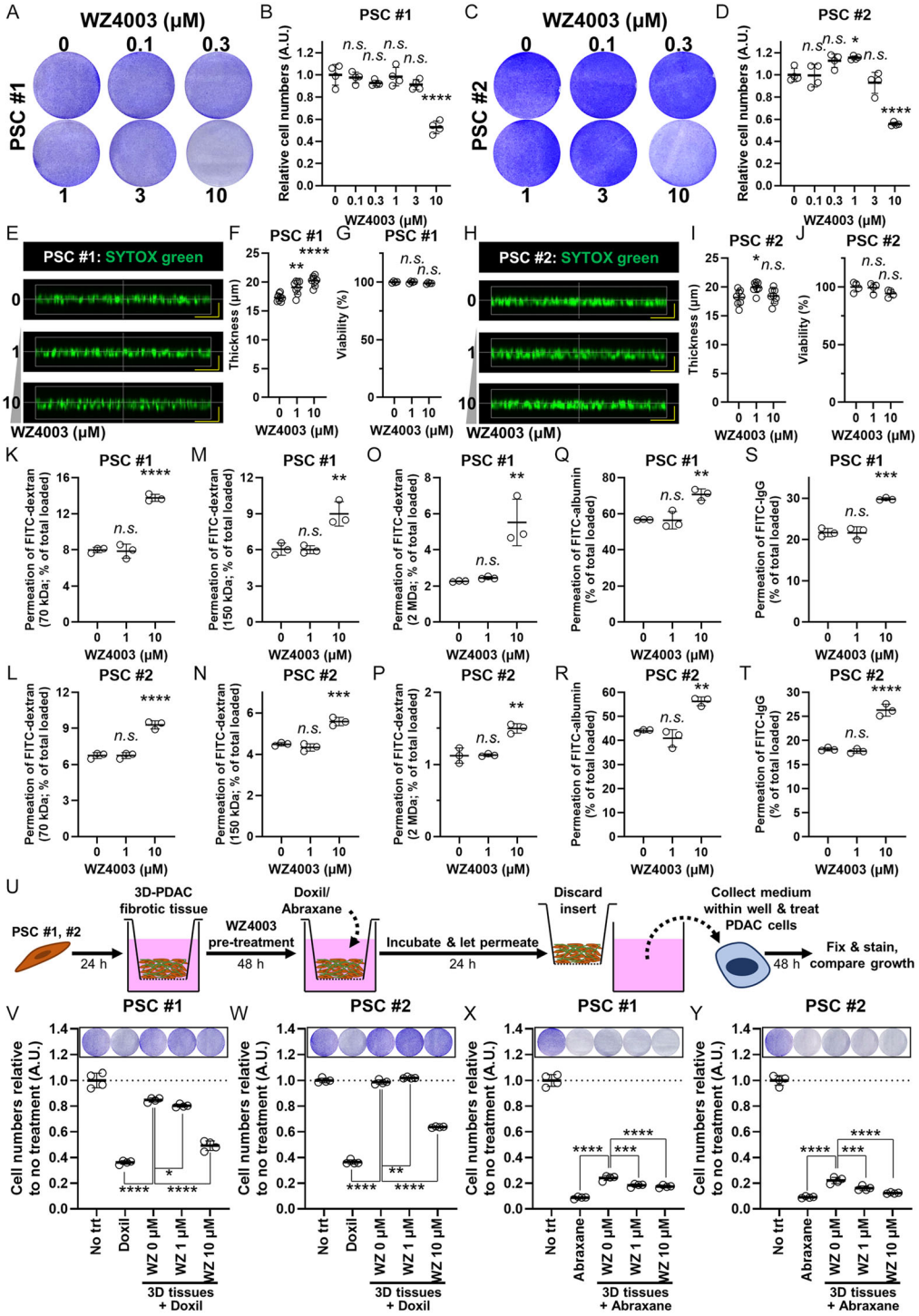

FIGURE 1 | Pharmacological inhibition of NUAK1/2 kinases enhances macromolecular permeability of 3D-PDAC fibrotic tissues. (A–D) Effect of the NUAK1/2 inhibitor WZ4003 on the proliferation of pancreatic stellate cells (PSC). Representative crystal violet stains are shown in (A,C). In (B,D), crystal violet was quantified after extraction with acetic acid via measurement of absorbance at 590 nm (A590), which is the absorbance maximum of crystal violet. (E–J) Representative 3D-reconstructed images (E,H) and measured thickness (F,G) as well as viability (G,J) of WZ4003-treated 3D-PDAC fibrotic tissues. $n = 8$ and $n = 4$ for thickness and viability measurements, respectively. Scale bars = 100 μm (horizontal) and 20 μm (vertical) in (E) and (H). (K–P) Permeability of WZ4003-treated 3D-PDAC fibrotic tissues to fluorescein isothiocyanate (FITC)-labeled dextran with average molecular weights of 70 kDa (K,L), 150 kDa (M,N), or 2000 kDa (O,P). (Q,R) Permeability of WZ4003-treated 3D-PDAC fibrotic tissues to FITC-labeled albumin. (S,T) Permeability of WZ4003-treated 3D-PDAC fibrotic tissues to FITC-labeled IgG. (U) Schematic depiction of assay assessing therapeutic effect of permeated clinical nanomedicines on PDAC cancer cells. (V–Y) Effect of Doxil (V,W) and Abraxane (X,Y) which permeated the 3D-PDAC fibrotic tissues on MiaPaCa-2 proliferation was compared to direct administration of the respective nanomedicine (second column). Cell numbers are shown relative to untreated MiaPaCa-2 cells (No trt; first column). Insets depict representative crystal violet stains. One-way analysis of variance (ANOVA) with *post hoc* Dunnett's multiple comparisons test was performed with 0 μM as the reference condition, and *n.s.*, *, **, ***, and **** denote not significant, $p < 0.05$, $p < 0.01$, $p < 0.001$, and $p < 0.0001$, respectively.

(Figure 1V–Y, second versus third column). The effect of interposed 3D-PDAC fibrotic tissues was less pronounced for Abraxane than Doxil, despite the larger nominal size of Abraxane (~130 nm in diameter) compared to Doxil (~100 nm) [19]. This may reflect the propensity of Abraxane to rapidly dissociate into smaller albumin-bound paclitaxel complexes [19] and/or its effect directly on fibrotic tissues [20]. Importantly, consistent with improved macromolecular permeability by WZ4003, pretreatment of 3D-PDAC fibrotic tissues with WZ4003 enhanced therapeutic effect of Doxil and Abraxane (Figure 1V–Y, third versus fourth and fifth columns).

2.2 | NUAK1/2 Inhibition Diminishes Myofibroblastic Differentiation of PSCs and Improves Macromolecular Permeability through Regulation of Collagen I Expression

PSCs become activated into αSMA-positive and collagen I-producing myofibroblasts in the PDAC microenvironment [4]. Motivated by a previous report showing regulation of myofibroblasts by NUAK1/2 [11], we wondered whether WZ4003 inhibits myofibroblastic differentiation of PSCs. Indeed, 10 μM WZ4003 decreased expression of αSMA protein (Figure 2A–C) and mRNA (Figure S2A,B). Collagen I expression in PSCs cultured in 2D (Figure 2D–F) as well as in 3D-PDAC fibrotic tissues (Figure 2G–I) was also diminished by 10 μM WZ4003. Similar reductions in αSMA (Figure S1K–M) and collagen I (Figure S1N–P) protein expression by 10 μM WZ4003 also were seen in prPSCs. Of the genes encoding collagen I, a triple helix generally consisting of two α1 chains encoded by *COL1A1* and one α2 chain encoded by *COL1A2* [23], 10 μM WZ4003 decreased *COL1A1* mRNA (Figure S2C,D), but its effect on *COL1A2* mRNA expression was comparatively weak (Figure S2E,F).

To assess whether decreased αSMA and/or collagen I is responsible for enhanced macromolecular permeability by WZ4003, we constructed 3D-PDAC fibrotic tissues with PSCs treated either with a control siRNA or an siRNA targeting the gene encoding αSMA, *ACTA2* (siACTA2), or siRNAs targeting *COL1A1* (siCOL1A1), *COL1A2* (siCOL1A2), or a 1:1 mixture of siCOL1A1 and siCOL1A2 (siCOL1A1 + 2) (Figure S3A–F). None of the siRNA treatments consistently affected PSC growth in 2D (Figure 2J–M) or diminished 3D-PDAC fibrotic tissue thickness (Figure 2N–Q). Interestingly, despite successful knockdown of *ACTA2* (Figure S3A,B), permeability of 3D-PDAC fibrotic tissues to 2000 kDa FITC-dextran was unaltered (Figure 2R,S). In contrast, knockdown of collagen I genes enhanced permeability of 3D-PDAC fibrotic tissues to 2000 kDa FITC-dextran (Figure 2T,U). These results suggest that downregulation of collagen I, but not αSMA, contributes to enhanced macromolecular permeability by WZ4003.

Notably, we found that siCOL1A1 + 2 downregulated *ACTA2* expression (Figure S2G,H), while siACTA2 did not affect *COL1A1* or *COL1A2* expression (Figure S2I–L). Consistently, at the protein level, both siACTA2 and siCOL1A1 + 2 diminished αSMA expression (Figure S2M–O), but only siCOL1A1 + 2 diminished collagen I expression by PSCs (Figure S2P–R). These results altogether suggest that NUAK1/2 inhibition via WZ4003 downregulates collagen I expression to enhance macromolecular permeability and diminish αSMA-positive myofibroblastic differentiation of PSCs.

2.3 | NUAK2 Knockdown Enhances Macromolecular Permeability of 3D-PDAC Fibrotic Tissues

WZ4003 is reportedly highly specific to NUAK1/2 with little activity even against closely related AMPK-related kinase family members. However, it inhibits both NUAK isoforms, albeit with a relatively lower IC_{50} value reported for NUAK1 ($IC_{50} = 20$ nm) versus NUAK2 ($IC_{50} = 100$ nm) [16]. To further establish NUAK1/2 involvement and assess the relative contributions of the two isoforms in the fibrotic barrier, we performed isoform-specific knockdown of NUAK1 and NUAK2 in PSCs (Figure S3G–J). Interestingly, treatment with an siRNA targeting NUAK2 (siNUAK2), but not siNUAK1, decreased collagen I expression in PSCs (Figure 3A–C). Collagen I expression in prPSCs was also decreased by siNUAK2, but not siNUAK1 (Figure S4A–C). Consistently, only siNUAK2 downregulated *COL1A1* mRNA expression (Figure 3D,E). As with WZ4003, the effect of siNUAK2 on *COL1A2* mRNA expression seemed somewhat weaker (Figure 3F,G).

Neither siNUAK1 nor siNUAK2 affected PSC growth in 2D (Figure 3H,I) or diminished 3D-PDAC fibrotic tissue thickness (Figure 3J,K). Nonetheless, siNUAK2 enhanced permeability to 2000 kDa FITC-dextran, while siNUAK1 did not to a statistically significant extent (Figure 3L,M). These results suggest that of the two isoforms, NUAK2 is more strongly involved in fibrotic barrier generation.

2.4 | NUAK Kinases Function Independently of YAP and TGFβ-SMAD2/3 Pathways in PSCs

Coordinated activity of the transcriptional regulator YAP and the TGFβ pathway transcription factors SMAD2/3 is implicated in organ fibrosis [8] and more specifically the generation of the fibrotic PDAC tumor microenvironment [10]. Interestingly, NUAK kinases have been previously identified as transcriptional targets of YAP signaling and demonstrated to regulate YAP activity [8, 12]. NUAK1/2 is also induced by TGFβ signaling and reciprocally regulates TGFβ-SMAD2/3 signaling pathway output [8, 11]. We thus wondered whether the effects of targeting NUAK1/2 were related to YAP and/or TGFβ-SMAD2/3 signaling.

To assess this, we treated PSCs with siRNAs against YAP (encoded by *YAP1*; siYAP1), SMAD2 (siSMAD2), SMAD3 (siSMAD3), or a 1:1 mixture of siSMAD2 and siSMAD3 (siSMAD2 + 3) (Figure S3K–P). PSC growth in 2D was mildly diminished by siYAP1 (Figure S5A,B). In contrast, siSMAD2, siSMAD3, or siSMAD2 + 3 did not consistently affect PSC growth (Figure S5C,D). None of the siRNAs affected 3D-PDAC fibrotic tissue thickness consistently in the two PSC cell lines tested (Figure S5E–H), but siYAP1, in line with our previous report [9], and siSMAD2, but not siSMAD3, enhanced permeability of 3D-PDAC fibrotic tissues to 2000 kDa FITC-dextran (Figure S5I–L). Consistent with the notion that regulation of collagen I expression by PSCs is important for macromolecular permeability, siYAP1, siSMAD2, siSMAD3, and siSMAD2 + 3 all attenuated collagen I expression (Figure S5M–T). Notably, siSMAD2 more strongly attenuated collagen I expression than siSMAD3, consistent with its stronger enhancement of macromolecular permeability (Figure S5Q–T).

Surprisingly, however, siYAP1, siSMAD2, siSMAD3, and siSMAD2 + 3 all failed to decrease NUAK1 (Figure 4A–D) or NUAK2 (Figure 4E–H) expression. This is in contrast to previous

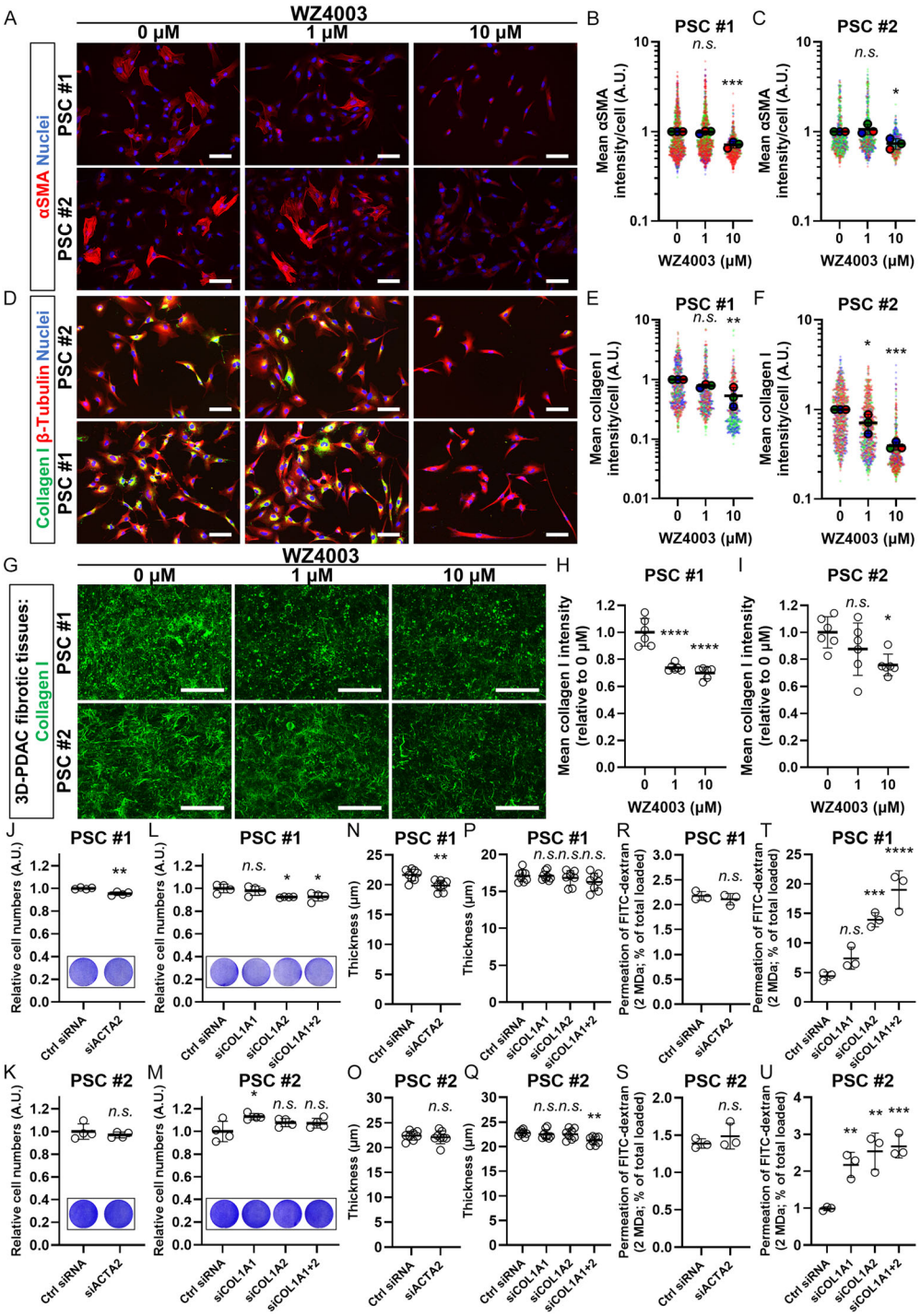

FIGURE 2 | NUAK1/2 inhibition diminishes collagen I expression to enhance macromolecular permeability of 3D-PDAC fibrotic tissues. (A) Representative immunofluorescent staining for αSMA (red) in WZ4003-treated PSCs. Nuclei (blue) were stained with Hoechst 33342. (B,C) Quantification of mean αSMA fluorescence per cell in WZ4003-treated PSCs per cell was quantified using CellProfiler [21] in WZ4003-treated PSCs. Aggregated data for three independently performed experiments are shown in distinct colors as superplots [22]: small data points in the background demonstrate quantified values of individual cells, and large data points in the foreground show the per experiment mean, together with error bars indicating standard deviation (SD) of the means. (D) Immunofluorescent staining for collagen I (green) and β-tubulin (red) in WZ4003-treated PSCs. Nuclei (blue) were stained with Hoechst 33342. (E,F) Mean collagen I fluorescence per cell in WZ4003-treated PSCs. (G) Maximum intensity projection images of WZ4003-treated 3D-PDAC fibrotic tissues immunofluorescently stained for collagen I. (H,I) Quantification of mean collagen I fluorescence of WZ4003-treated 3D-PDAC fibrotic tissues. (J,K) Effect of siRNA targeting *ACTA2* (siACTA2) versus a control (ctrl) siRNA on PSC growth. (L,M) Effect of siRNAs targeting *COL1A1* (siCOL1A1), *COL1A2* (siCOL1A2), or a 1:1 mixture of siCOL1A1 and siCOL1A2 (siCOL1A1 + 2) on PSC growth. (N–Q) Effect of siACTA2 (N,O), siCOL1A1, siCOL1A2, or siCOL1A1 + 2 (P,Q) on 3D-PDAC fibrotic tissue thickness. (R–U) Permeability to 2000 kDa FITC-dextran of 3D-PDAC fibrotic tissues constructed from PSCs treated with siACTA2 (R,S), siCOL1A1, siCOL1A2, or siCOL1A1 + 2 (T,U) compared to ctrl siRNA. One-way ANOVA with post hoc Dunnett's multiple comparison test was performed with 0 μM or ctrl siRNA as the reference condition, and *n.s.*, *, **, ***, and **** denote not significant, $p < 0.05$, $p < 0.01$, $p < 0.001$, and $p < 0.0001$, respectively.

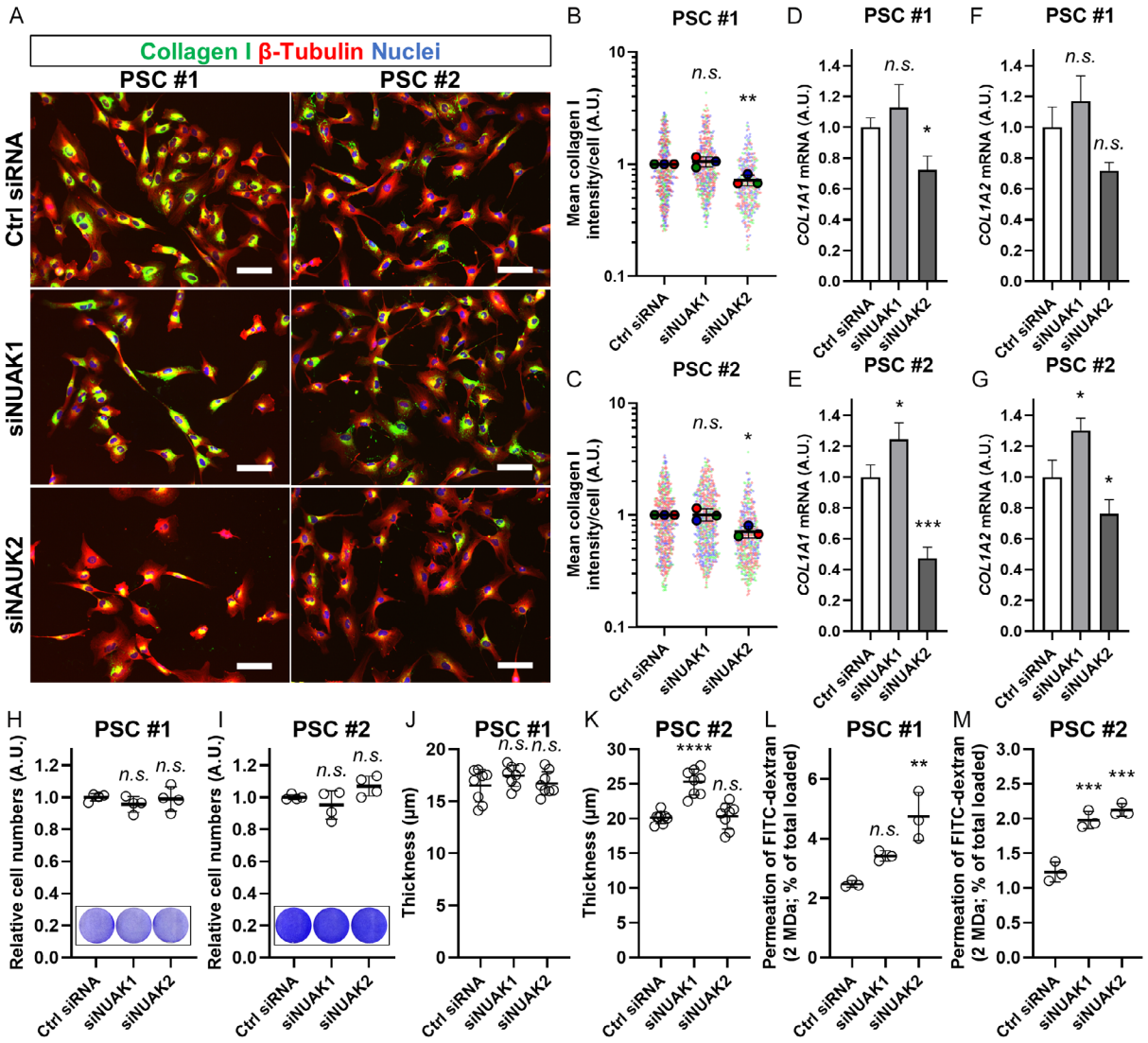

FIGURE 3 | *NUAK2* knockdown enhances macromolecular permeability of 3D-PDAC fibrotic tissues. (A) Immunofluorescent staining for collagen I (green) and *β*-tubulin (red) in PSCs treated with siRNAs targeting *NUAK1* (siNUAK1), *NUAK2* (siNUAK2), or ctrl siRNA. Nuclei (blue) were stained with Hoechst 33342. Scale bars = 100 μm. (B,C) Mean collagen I fluorescence per cell in PSCs upon knockdown of *NUAK1* or *NUAK2*. (D–G) *COL1A1* (D,E) or *COL1A2* (F,G) mRNA expression in PSCs treated with ctrl siRNA, siNUAK1, or siNUAK2. $n = 3$ biological replicates. (H,I) Effect of *NUAK1* or *NUAK2* knockdown on the proliferation of PSCs. (J–M) Thickness (J,K) and permeability to 2000 kDa FITC-dextran (L,M) of 3D-PDAC fibrotic tissues constructed from PSCs treated with ctrl siRNA, siNUAK1, or siNUAK2. $n = 8$ thickness measurements. One-way ANOVA with post hoc Dunnett's multiple comparisons test was performed with ctrl siRNA as the reference condition, and *n.s.*, *, **, ***, and **** denote not significant, $p < 0.05$, $p < 0.01$, $p < 0.001$, and $p < 0.0001$, respectively.

reports identifying NUAK1/2 as downstream transcriptional targets and effectors of YAP [8, 24] and TGF*β*/SMAD [8, 11] signaling (Figure 4I) and suggests that YAP and SMAD2/3 are dispensable for NUAK1/2 expression in PSCs. Given that NUAK1/2 has also been reported to reciprocally regulate YAP [8, 24] and TGF*β*/SMAD [8, 11] signaling (Figure 4J), we wondered whether NUAK1/2 may function as upstream regulators instead. To this end, we assessed the effect of WZ4003 on the expression of *CTGF*, a well-established transcriptional target of YAP [25] and TGF*β*/SMAD [26, 27] (Figure 4K–N). However, WZ4003 did not affect *CTGF* expression (Figure 4O,P), suggesting that YAP and TGF*β*/SMAD activity were not significantly altered. These results altogether suggest that, in PSCs, NUAK1/2 largely functions independently of YAP or SMAD2/3 activity, but converges upon the regulation of collagen I expression to promote fibrotic barrier generation.

2.5 | Targeting of NUAK2 Diminishes Stress Fibers in PSCs to Attenuate Collagen I Expression in PSCs and Enhances Macromolecular Permeability of 3D-PDAC Fibrotic Tissues

We next sought to elucidate the mechanisms by which NUAK2 targeting diminishes collagen I expression by PSCs and enhances macromolecular permeability. NUAK2 is recruited to actin stress fibers, where it physically interacts with and counteracts MYPT1, the regulatory subunit of myosin regulatory light chain phosphatase, to inhibit stress fiber disassembly [28]. Indeed, phalloidin staining of PSCs revealed a prominent diminution of actin stress fibers by WZ4003 (Figure 5A–C), an effect also confirmed in prPSCs (Figure S6A–C). Moreover, siNUAK2 decreased phalloidin staining of PSCs compared to control siRNA, in contrast to

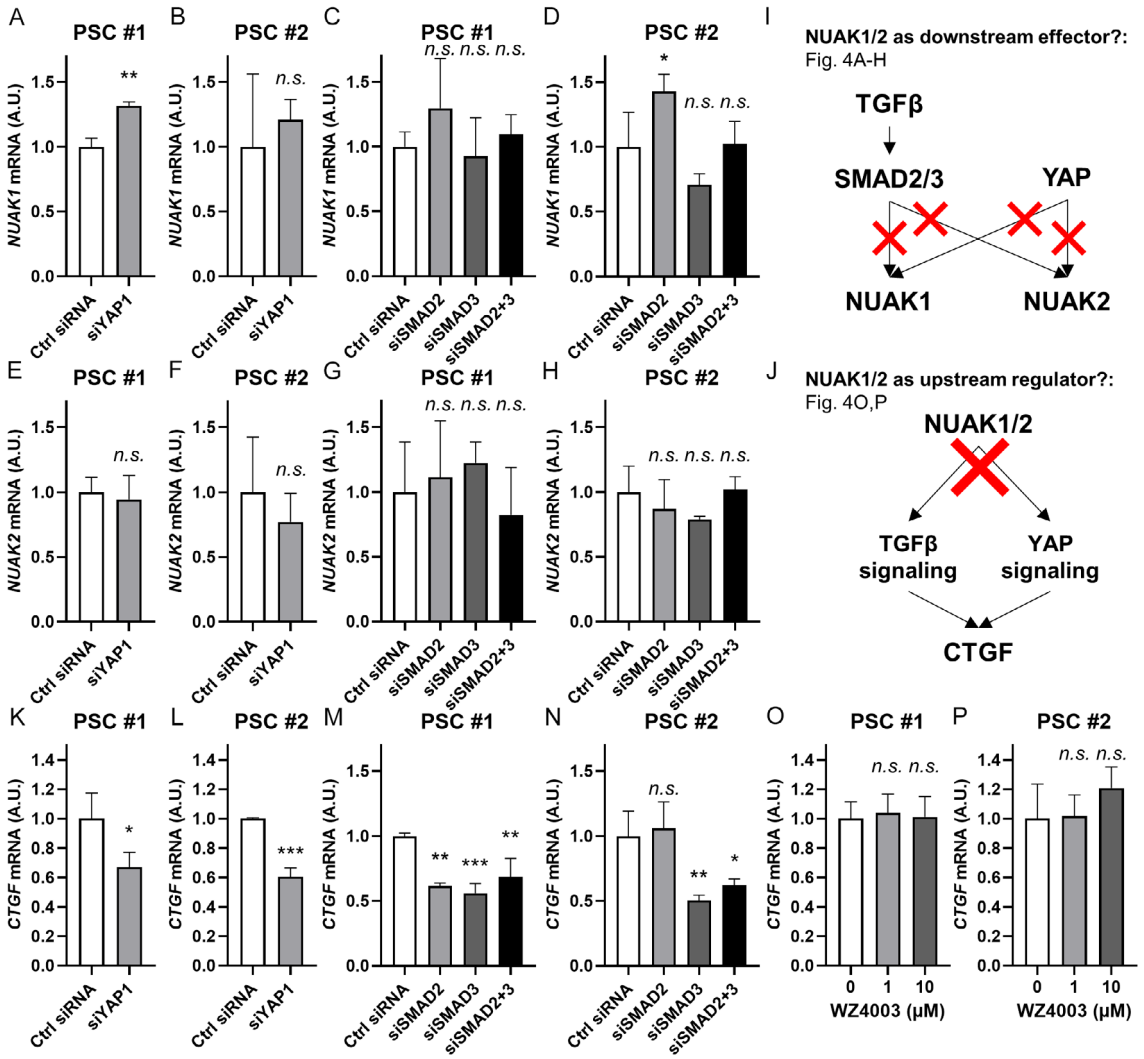

FIGURE 4 | *NUAK* kinases function independently of YAP and TGFβ-SMAD2/3 pathways in PSCs. (A,B) *NUAK1* mRNA expression in PSCs treated with an siRNA targeting YAP1 (siYAP). (C,D) *NUAK1* mRNA expression in PSCs treated with an siRNA targeting SMAD2 (siSMAD2), SMAD3 (siSMAD3), or a 1:1 mixture of siSMAD2 and siSMAD3 (siSMAD2 + 3) versus ctrl siRNA. (E,F) *NUAK2* mRNA expression upon siYAP1 treatment of PSCs. (G,H) *NUAK2* mRNA expression upon siSMAD2, siSMAD3, or siSMAD2 + 3 treatment of PSCs. (I,J) Schematic figure of the reported role of NUAK1/2 as downstream effectors (I) or upstream regulators (J) of TGFβ-SMAD2/3 and YAP signaling. Red crosses indicate roles unobserved in our data. (K–P) *CTGF* mRNA expression in PSCs upon siYAP1 (K,L) or siSMAD2, siSMAD3, and siSMAD2 + 3 treatment (M,N). (O,P) *CTGF* mRNA expression in WZ4003-treated PSCs. $n = 3$ biological replicates. Student's unpaired t-test with Welch's correction was performed in (A), (B), (E), (F), (K), and (L). In all other graphs, one-way ANOVA with post hoc Dunnett's multiple comparisons test was performed with ctrl siRNA or 0 μM as the reference condition. In all graphs, *n.s.*, *, **, and *** denote not significant, $p < 0.05$, $p < 0.01$, and $p < 0.001$, respectively.

siNUAK1 which demonstrated a comparatively weak effect (Figure 5D–F). Phalloidin staining in prPSCs was also reduced by siNUAK2, but not consistently by siNUAK1 (Figure S6D–F).

Motivated by a report of reductions in collagen I expression by disassembly of the actin cytoskeleton in dermal fibroblasts [29], we next sought to establish whether a similar mechanism operates in PSCs and is responsible for the enhancement of macromolecular permeability observed upon NUAK2 targeting. As myosin II and its activation by myosin light chain kinase (MLCK) is indispensable for stress fiber assembly and maintenance [30], we used the myosin II inhibitor blebbistatin and MLCK inhibitor ML-7 to induce stress fiber disassembly. Indeed, phalloidin staining of blebbistatin- or ML-7-treated PSCs and prPSCs confirmed a dose-dependent diminution of actin stress fibers (Figures 5G–I, S7A–C and S8A–F), accompanied by decreased collagen I expression (Figures 5J–L, S7D–F, and S8D–F). Blebbistatin also diminished collagen deposition in 3D-PDAC fibrotic tissues (Figure 5M–O). Though both blebbistatin and ML-7 at 10 μM suppressed PSC growth in 2D (Figures 5P,Q and S7G,H), 3D-PDAC fibrotic tissue thickness was not decreased at any of the concentrations tested (Figures 5R,S and S7I,J). Nonetheless, blebbistatin and ML-7 dose-dependently enhanced macromolecular permeability of 3D-PDAC fibrotic tissues (Figures 5T,U and S7K,L). Similar enhancement of macromolecular permeability by blebbistatin and ML-7 was also observed in 3D-PDAC fibrotic tissues constructed from prPSCs (Figure S8G–P). These results together suggest that stress fiber disassembly may contribute to the therapeutic effects of targeting NUAK2.

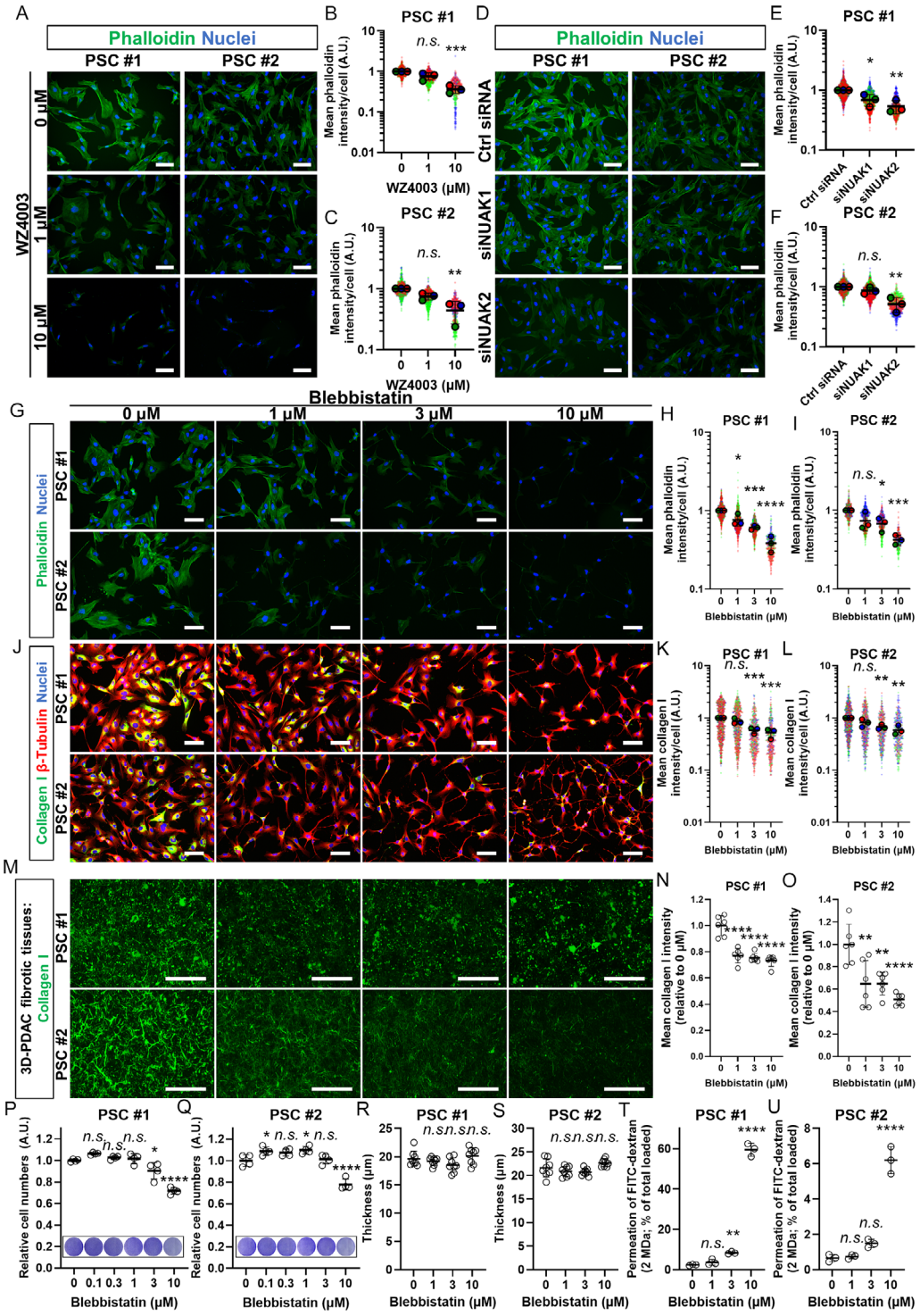

FIGURE 5 | Targeting of NUAK2 diminishes stress fibers to attenuate collagen I expression in PSCs and enhance macromolecular permeability of 3D-PDAC fibrotic tissues. (A) Staining of filamentous actin with phalloidin (green) in WZ4003-treated PSCs. Nuclei (blue) were stained with Hoechst 33342. (B,C) Mean phalloidin fluorescence per cell in WZ4003-treated PSCs. (D) Phalloidin (green) and Hoechst 33342 (blue) staining of PSCs treated with ctrl siRNA, siNUAK1, or siNUAK2. (E,F) Mean phalloidin fluorescence per cell in PSCs treated with siNUAK1 or siNUAK2. (G) Phalloidin (green) and Hoechst 33342 (blue) staining of PSCs treated with the myosin II inhibitor blebbistatin. (H,I) Mean phalloidin fluorescence per cell in blebbistatin-treated PSCs. (J) Blebbistatin-treated PSCs were immunofluorescently stained for collagen I (green) and β-tubulin (red). Nuclei (blue) were stained with Hoechst 33342. (K,L) Mean collagen I fluorescence per cell in blebbistatin-treated PSCs. (M) Maximum intensity projection images of blebbistatin-treated 3D-PDAC fibrotic tissues immunofluorescently stained for collagen I. (N,O) Quantification of mean collagen I fluorescence of blebbistatin-treated 3D-PDAC fibrotic tissues. (P,Q) Effect of blebbistatin on the proliferation of PSCs. (R–U) Thickness (R,S) and permeability to 2000 kDa FITC-dextran (T,U) of blebbistatin-treated 3D-PDAC fibrotic tissues. $n = 8$ thickness measurements. Scale bars = 100 μm. One-way ANOVA with post hoc Dunnett's multiple comparisons test was performed with 0 μM or ctrl siRNA as the reference condition, and *n.s.*, *, **, ***, and **** denote not significant, $p < 0.05$, $p < 0.01$, $p < 0.001$, and $p < 0.0001$, respectively.

2.6 | Combined Targeting of NUAK2 and ROCK2 Further Enhances Macromolecular Permeability of 3D-PDAC Fibrotic Tissues Compared to Targeting of Either Kinase Alone

NUAK2 was previously shown to regulate actin stress fibers independently of the myosin regulatory light chain kinase Rho-associated kinase (ROCK) in HeLa cells [28]. Since we recently discovered ROCK2 involvement in the PDAC fibrotic barrier [9], we wondered whether targeting both NUAK2 and ROCK2 in PSCs would further enhance macromolecular permeability. As expected, knockdown of NUAK2, *ROCK2*, or the combination of both (Figure S3I,J,Q,R) attenuated phalloidin staining (Figure 6A–C) and collagen I expression (Figure 6D–F) in PSCs. Addition of siROCK2 did not further attenuate phalloidin staining, but showed a trend toward further reduction of collagen I more than siNUAK2 alone (Figure 6E,F).

Encouraged by the above results, we finally asked whether this combination further enhances macromolecular permeability of 3D-PDAC fibrotic tissues compared to targeting NUAK2 or ROCK2 alone. Although the co-administration of WZ4003 together with the ROCK inhibitor fasudil at various concentrations revealed that this combination was not globally synergistic, the combination of both inhibitors at 10 μM markedly enhanced macromolecular permeability (Figure 6G–J). The benefit of combined targeting of NUAK2 with ROCK2 was further corroborated by the finding that additional treatment with the ROCK2-isoform-specific inhibitor KD025 results in higher macromolecular permeability in 3D-PDAC fibrotic tissues constructed from PSCs treated with siNUAK2 versus control siRNA (Figure 6K,L).

3 | Discussion

Using PDAC patient-derived primary and immortalized PSCs, we assessed the involvement of the AMPK-related kinases NUAK1/2 to gain a deeper understanding of the mechanisms driving fibrotic barrier generation in PDAC. We demonstrate that targeting NUAK2 enhances macromolecular drug delivery through 3D-PDAC fibrotic tissues. Several previous studies have investigated the benefits of NUAK inhibition in suppressing PDAC tumor cell proliferation and therapeutic resistance [32–35], but this is the first to show its role in the fibrotic barrier to the best of our knowledge. Mechanistically, NUAK2 inhibition diminished collagen I expression by inducing actin stress fiber disassembly in PSCs. 3D-PDAC fibrotic tissue thickness and viability were however not significantly diminished, suggesting that NUAK2 inhibition is not stroma ablative. Numerous NUAK inhibitors have been developed with varying levels of potency and specificity [7]. Unfortunately, in contrast to NUAK1-specific inhibitors, such as HTH-01-015 with 1000-fold lower affinity to NUAK2, NUAK2-specific inhibitors have yet to be reported [7, 36].

We initially focused on NUAK1/2 given their involvement in YAP and TGFβ signaling [8, 11, 12], both pathways shown to be important drivers of fibrosis in PDAC [9, 10]. However, we could not confirm regulation of NUAK1/2 expression by YAP, SMAD2, or SMAD3. We furthermore did not observe altered expression of *CTGF*, a canonical transcriptional target of both YAP and TGFβ/SMAD, upon *NUAK1/2* knockdown in PSCs. Overall, this suggests that NUAK1/2 largely functions independently of YAP or TGFβ/SMAD pathways in PSCs. Although the mechanisms regulating *NUAK1/2* expression remain incompletely understood, the involvement of transcription factors other than YAP or SMAD2/3, such as nuclear factor kappa B [33], has recently also been reported. Differential expression of the two NUAK isoforms across various adult tissues [6] also suggests there may be cell type-specific differences in transcriptional regulation of *NUAK1/2*. A detailed investigation of the mechanisms regulating NUAK expression in PSCs is thus warranted.

We recently reported that ROCK2 inhibition is effective in overcoming the PDAC fibrotic barrier [9]. Herein, we found that inhibition of NUAK2 and ROCK2 both converge upon stress fiber disassembly to regulate collagen I expression in PSCs and that combined targeting of NUAK2 and ROCK2 enhances macromolecular permeability more than either targeted alone. Stress fiber dynamics thus seem an important determinant of fibrotic PSC phenotype and macromolecular permeability of fibrotic tissues. Interestingly, while αSMA is known to be incorporated into stress fibers to direct a contractile, myofibroblastic phenotype [37], *ACTA2* knockdown did not affect collagen I expression or macromolecular permeability. Instead, our data indicate that diminished αSMA expression upon NUAK2 targeting is a downstream consequence of reduced collagen I. Detailed analyses of the signaling pathways governing stress fibers may yield further information regarding the mechanisms driving fibrotic barrier generation.

Importantly, the present study highlights the utility of 3D cell culture models in studying the fibrotic PDAC tumor microenvironment. Commonly used cell-line-derived xenograft models of PDAC often fail to show appreciable levels of fibrosis [38]. While genetically engineered mouse models and patient-derived xenografts models of PDAC are often better at recapitulating fibrosis, they are time-consuming and expensive and show great variability [39]. In contrast, 3D cell culture models are relatively easy, cheap, and highly reproducible and thus may complement in vivo studies and expedite drug evaluation and delivery. Indeed, as demonstrated in the present study, 3D cell culture models are potentially useful in screening of drug combinations that effectively remodel the fibrotic barrier across a range of concentrations, an assessment otherwise difficult and costly if performed in vivo.

In summary, we demonstrated that NUAK2 signaling in PSCs promotes the fibrotic barrier to macromolecular drug delivery in PDAC through regulation of actin stress fibers. Our data advance the understanding of the molecular and cellular mechanisms driving fibrotic barrier generation and provide the foundation for future assessment in vivo of targeting NUAK2, and the potential for combination with ROCK2 inhibition, to augment efficacy of macromolecular drugs and to improve treatment outcomes in PDAC.

4 | Experimental Section

4.1 | Cell Culture and Reagents

Primary PSCs, prPSC #1 and prPSC #2, and the immortalized PSC cell-lines, PSC #1 and PSC #2, were established under the approval by the Ethics Committee of Tohoku University Graduate School of Medicine (article#: 2023-1-730) and have previously been characterized in 3D-PDAC fibrotic tissues [9, 13, 15]. Briefly, prPSCs were established from patients who underwent surgery for pancreatic cancer, and immortalization was performed by the retrovirus-mediated gene transfer of simian virus 40 (SV40) T antigen and

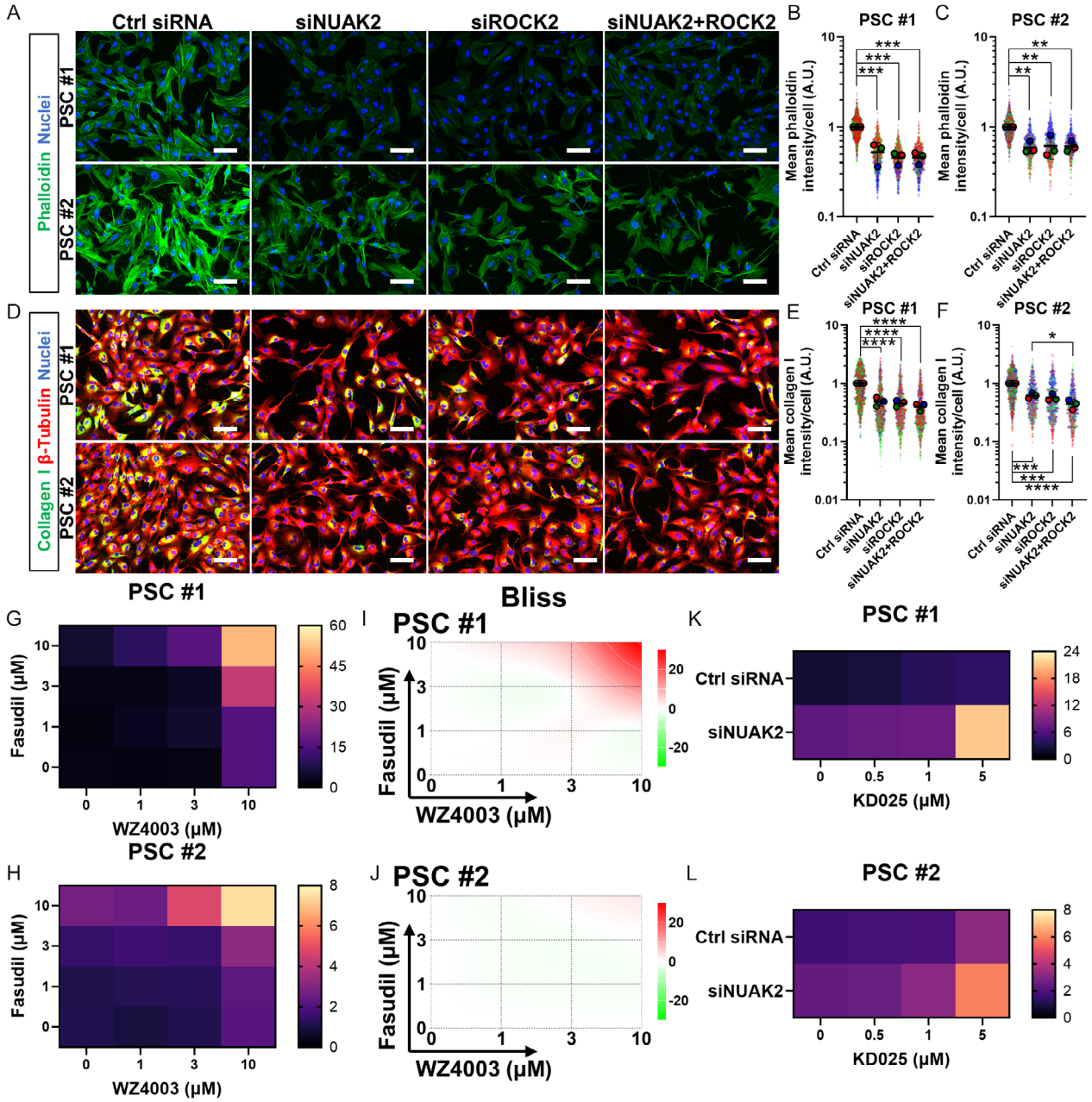

FIGURE 6 | Combined targeting of NUAK2 and ROCK2 further enhances macromolecular permeability of 3D-PDAC fibrotic tissues compared to targeting of either kinase alone. (A) Phalloidin (green) and Hoechst 33342 (blue; nuclei) staining of PSCs treated with siNUAK2, an siRNA targeting ROCK2 (siROCK2), or a 1:1 mixture of siNUAK2 and siROCK2 (siNUAK2+ROCK2). (B,C) Mean phalloidin fluorescence per cell in PSCs treated as in (A). (D) Immunofluorescent staining for collagen I (green) and β-tubulin (red) in PSCs treated with siNUAK2, siROCK2, or siNUAK2+ROCK2. Nuclei (blue) were stained with Hoechst 33342. (E,F) Mean collagen I fluorescence per cell in PSCs treated as in (D). (G,H) Heatmap showing permeability to 2000 kDa FITC-dextran of 3D-PDAC fibrotic tissues treated with a combination of WZ4003 and the ROCK inhibitor fasudil at various concentrations. Values indicate % of total loaded. (I,J) Based on the data in (G) and (H), respectively, Bliss synergy scores and p-values were calculated using SynergyFinder Plus [31]. Higher positive values (red) indicate strong synergy; negative values (green) indicate antagonism. $p = 0.122$ and $p = 0.591$ for PSC #1 and #2, respectively. (K,L) Heatmap showing permeability to 2000 kDa FITC-dextran of 3D-PDAC fibrotic tissues constructed from PSCs treated with siNUAK2, then treated with the ROCK2-specific inhibitor KD025. Scale bars = 100 μm. In all graphs, one-way ANOVA with post hoc Tukey's multiple comparison test was performed. *, **, ***, and **** denote $p < 0.05$, $p < 0.01$, $p < 0.001$, and $p < 0.0001$, respectively; otherwise, differences were not statistically significant.

human telomerase reverse transcriptase (hTERT), as previously described [40]. MiaPaCa-2 cells were obtained from American Type Cell Collection (Manassas, VA, USA). PSCs were maintained in Dulbecco's modified Eagle medium (Gibco/Thermo Fisher Scientific, Eugene, MA, USA) supplemented with 10% (v/v) fetal bovine serum, 1×GlutaMAX (Gibco/Thermo Fisher Scientific), 50 U mL^{-1} penicillin, and 50 μg mL^{-1} streptomycin. MiaPaCa-2 cells were cultured in Dulbecco's modified Eagle medium supplemented with 10% FBS, 50 U mL^{-1} penicillin, and 50 μg mL^{-1} streptomycin.

Blebbistatin, fasudil, KD025, ML-7, and WZ4003 were all from Selleck Chemicals (Houston, TX, USA) and prepared as dimethyl

sulfoxide (DMSO) solutions. Due to reported phototoxicity and photoinactivation of blebbistatin [41], all experiments involving blebbistatin were performed in the dark. Clinical nanomedicines used in this study, Doxil and Abraxane, were from Janssen Pharmaceutical K.K. (Tokyo, Japan) and Taiho Pharmaceutical Co., Ltd. (Tokyo, Japan), respectively. Abraxane was prepared as a 5 mg mL^{-1} solution in physiological saline (Otsuka Pharmaceutical Co., Ltd., Tokyo, Japan) according to manufacturer instructions.

4.2 | Cell Proliferation Assay

PSCs or prPSCs were seeded onto 6-well plates (BD Falcon/Corning, Corning, NY, USA; 1×10^5/well) or onto 24-well plates (BD Falcon/Corning; 2×10^4/well) in quadruplicates. To assess the effect of siRNAs on cell growth, cells were transfected with the respective siRNA 24 h postcell seeding as described below. The culture medium was replaced every day, together with pharmacological inhibitors as necessary. Plates were fixed 72 h postcell seeding with 4% (w/v) paraformaldehyde (PFA) in phosphate-buffered saline (PBS) for 5 min at room temperature (RT) after being washed once briefly with PBS. Plates were then washed once briefly with PBS and then stained with 0.5% (w/v) aq. crystal violet (Tokyo Chemical Industry Co., Ltd., Tokyo, Japan) upon gentle rocking (20 min, RT). After removing the staining solution, plates were washed with water to remove any residual stain, and then completely dried. Stained 6-well plates were photographed using a handheld camera. Stained 24-well plates were quantified, as follows. To extract crystal violet, equal amounts of 10% (v/v) aq. acetic acid were applied to each well. After gently rocking the plates (20 min, RT) to complete extraction, 100 µL/well was collected and applied onto 96-well plates (Nunc/Thermo Fisher Scientific, Roskilde, Denmark). Absorbance (590 nm) was measured using TriStar2 LB942 (Berthold Technologies, Bad Wildbad, Germany). Relative cell numbers were obtained by dividing each absorbance value by the average of the control condition (0 µM condition for experiments involving pharmacological inhibitors, and ctrl siRNA for experiments involving siRNAs).

4.3 | Immunofluorescent Staining and Analysis

PSCs or prPSCs (2×10^4 cells) were seeded onto 15-mm glass-bottom dishes (Matsunami Glass Ind., Osaka, Japan) coated with collagen (Nitta Gelatin, Osaka, Japan; Cellmatrix Type I-C; 0.1 mg mL^{-1}, >30 min at 37°C). For knockdown experiments, cells were transfected with siRNAs prior to seeding onto glass-bottom dishes, as follows. First, cells (1×10^5 cells) were seeded onto 6-well plates. Then, siRNAs (10 nM) were transfected using Lipofectamine RNAiMAX (Invitrogen/Thermo Fisher Scientific, Carlsbad, CA, USA) 24 h after cell seeding. The siRNAs used in this study were predesigned (MISSION siRNA, Sigma–Aldrich) except for the control siRNA (ctrl siRNA; sense: GUACCGCACGUCAUUCGUAUC; anti-sense: UACGAAUGACGUGCGGUACGU) and siSMAD2 (sense: GAGCUAUACUAGAUAGCCUCA; anti-sense: AGGCUA UCUAGUAUAGCUCAU) which were obtained from Sigma Genosys (Tokyo, Japan). For the predesigned siRNAs, the respective IDs supplied by the manufacturer are as follows: siACTA2 (SASI_Hs01_00097016), siCOL1A1 (SASI_Hs02_00301842), siCOL1A2 (SASI_Hs02_00301848), siNUAK1 (SASI_Hs01_00188391), siNUAK2 (SASI_Hs01_00091747), siROCK2 (SASI_Hs01_00204251), siSMAD3 (SASI_Hs01_00208931), and siYAP1 (SASI_Hs01_00182402). Cells were harvested and seeded onto glass-bottom dishes 24 h after transfection. The culture medium was replaced daily. Pharmacological inhibitors were administered at the time of medium change.

Samples were fixed with 4% (w/v) PFA/PBS (1 min, RT) for immunofluorescent staining 72 h after cell seeding. Cells were then permeabilized with 0.2% (v/v) Triton X-100/PBS (5 min, RT) and blocked with Blocking One (Nacalai Tesque, Kyoto, Japan; 1–2 h, RT). Cells were then incubated with primary antibodies diluted in Blocking One (overnight [O/N], 4°C). The following primary antibodies were used in this study: β-tubulin (014-25041; Wako Pure Chemicals, Osaka, Japan; mouse monoclonal, clone: 10G10, 1/500 dilution) and collagen I (ab138492; Abcam, Cambridge, UK; rabbit monoclonal, clone: EPR7785, 1/1000 dilution). Following washing with PBS thrice, cells were incubated with the respective Alexa Fluor-labeled secondary antibodies (Molecular Probes/Thermo Fisher Scientific, Eugene, OR, USA; O/N, 4°C; 1/200 dilution) diluted in Blocking One. Visualization of stress fiber was performed by staining of filamentous actin with Phalloidin-iFluor 488 reagent (ab176753; Abcam, 1/1000 dilution) together with secondary antibody labeling. To stain α-smooth muscle actin (αSMA), anti-actin, α-smooth muscle-Cy3 antibody (C6198; Sigma–Aldrich; mouse monoclonal, clone: 1A4, 1/200 dilution) was used together with phalloidin, diluted in Blocking One. Cells were finally stained with Hoechst 33342 (Thermo Fisher Scientific, Waltham, MA, USA; 2 µg mL^{-1} in PBS; O/N, 4°C). After washing with PBS twice, cells were observed under a Keyence BZ-9000 or BZ-X810 fluorescence microscope (Osaka, Japan). Images were analyzed using CellProfiler [21] to obtain mean fluorescence intensity per cell.

4.4 | Generation of 3D-PDAC Fibrotic Tissues

3D-PDAC fibrotic tissues were constructed from PSCs and prPSCs as reported previously [9, 13]. Cells after trypsinization were incubated in Tris-buffered saline (pH 7.4) containing 0.04 mg mL^{-1} fibronectin (Sigma–Aldrich, St. Louis, MO, USA) and 0.04 mg mL^{-1} gelatin (Wako Pure Chemicals) upon gentle rocking (30 min, RT). Following brief centrifugation and resuspension in fresh culture media, PSCs (1×10^6 cells/insert) or prPSCs (5×10^5 cells/insert) were seeded on translucent (high pore density; 0.4 µm pores) cell culture inserts (BD Falcon/Corning) for 24-well plates (BD Falcon/Corning), coated with 0.12 mg mL^{-1} fibronectin. We have previously established that these cell seeding densities result in 3D-PDAC fibrotic tissues with a thickness of approximately 15–20 µm, which is within the clinically observed range of the distance that an intravenous drug must penetrate to locate a tumor target within the fibrotic human PDAC microenvironment [13]. Culture media were replaced every 24 h. Pharmacological inhibitors were administered to 3D-PDAC fibrotic tissues beginning from 24 h after cell seeding at the time of medium change.

To generate 3D-PDAC fibrotic tissues from PSCs with specific genes knocked down, siRNA transfections were performed prior to 3D tissue generation. PSCs seeded onto 100-mm culture dishes (BD Falcon/Corning) at a density of 6×10^5 cells/dish were transfected with siRNAs 24 h postcell seeding as described above.

PSCs were then harvested for generating 3D-PDAC fibrotic tissues 24 h after siRNA transfection.

4.5 | Fluorescent Staining of 3D-PDAC Fibrotic Tissues

After 3 days of culture, 3D-PDAC fibrotic tissues were fixed with 4% (w/v) PFA/PBS (5 min, RT) after washing with PBS once. Following fixation, 3D-PDAC fibrotic tissues were blocked with Blocking One (1–2 h, RT) and incubated with anti-collagen I antibody (ab138492; Abcam) diluted in Blocking One (1/1000 dilution; O/N, 4°C). After washing with PBS thrice, 3D-PDAC fibrotic tissues were incubated with the respective Alexa Fluor-labeled secondary antibodies diluted in Blocking One (1/200 dilution; O/N, 4°C). Finally, 3D-PDAC fibrotic tissues were stained with Hoechst 33342 (2 μg mL^{-1} in PBS; O/N, 4°C). After washing with PBS thrice, culture insert membranes were carefully excised using a scalpel and mounted on coverslips using fluorescent mounting medium (Dako/Agilent, Santa Clara, CA, USA). Samples were then observed under a BZ-X810 fluorescence microscope. Collagen network within the 3D-PDAC fibrotic tissues was visualized by obtaining a Z-stack of 0.3 μm slices to acquire a maximum intensity projection image using the BZ-H4A image analysis software (Keyence), which was then used to quantify mean fluorescence intensity in ImageJ (NIH, Bethesda, MD, USA).

4.6 | Thickness Measurements of 3D-PDAC Fibrotic Tissues

The thickness of 3D-PDAC fibrotic tissues was determined as previously reported [9, 13]. 3D-PDAC fibrotic tissues were fixed 72 h after 3D tissue generation with 4% (w/v) PFA/PBS (5 min, RT) after a brief wash once with PBS. After fixation, samples were washed with PBS thrice and permeabilized with 0.2% (v/v) Triton X-100/PBS (20 min, RT). Samples were then stained with SYTOX Green nucleic acid stain (Molecular Probes/Thermo Fisher Scientific; 0.2 μM; O/N, 4°C) to visualize cell nuclei. After washing with PBS thrice, culture insert membranes were carefully excised using a scalpel and mounted onto coverslips using fluorescent mounting medium (Dako/Agilent, Santa Clara, CA, United States). Samples were observed under a Keyence BZ-X810 fluorescence microscope, and Z-stack images of 0.5 μm slices were obtained. Acquired images were 3D-reconstituted, and the thickness was measured using the BZ-H4A image analysis software (Keyence).

4.7 | Assessment of the Viability of 3D-PDAC Fibrotic Tissues

The viability of 3D-PDAC fibrotic tissues was assessed in quadruplicates using the LDH cytotoxicity assay kit (Nacalai Tesque), which is based on the reduction of tetrazolium salt to formazan by lactate dehydrogenase (LDH) released from damaged cells.

Two days after 3D-PDAC fibrotic tissue generation, culture media were replaced (0.5 mL inside the insert and 1 mL in the well). Positive controls were prepared by lysing nontreated samples (0.4 mL culture media + 0.1 mL lysis solution inside the insert). After 30 min, culture media supernatants (100 μL) were collected from within the insert, applied onto 96-well plates (Nunc/Thermo Fisher Scientific), then mixed with substrate solution (100 μL). After incubating in the dark (20 min, RT), stop solution (50 μL) was added to terminate the reduction reaction. Absorbance (490 nm) was measured using TriStar2 LB942.

Cell viability relative to nontreated samples by the following formula: Relative cell viability = {1 − (absorbance of sample − absorbance of non-treated samples)/(absorbance of lysed samples − absorbance of non-treated samples)} × 100 (%).

4.8 | Assessment of the Macromolecular Permeability of 3D-PDAC Fibrotic Tissues

Macromolecular permeability of 3D-PDAC fibrotic tissues was assessed as previously described [9]. Three days after 3D-PDAC fibrotic tissue generation, culture media were replaced (0.45 mL inside the insert and 1 mL in the well). Respective fluorescently labeled macromolecules (50 μL; detailed below) were then gently loaded onto the inserts. Inserts were carefully removed and discarded after 24 h of incubation. Media within the wells were stored in the dark until measurement. Samples (100 μL) were loaded onto clear 0.5 mL tubes (Greiner Bio-One, Kremsmünster, Austria) and measured using a DeNovix DS-11 fluorometer (Wilmington, DE, USA). Concentration of the macromolecule in the sample was determined from a standard curve obtained using known concentrations of the macromolecule diluted in culture media. The percentage of macromolecules that permeated the 3D-PDAC fibrotic tissues was calculated as $C/C_\infty \times 100$, where C is the measured sample concentration and C_∞ is the theoretical concentration without 3D tissues at equilibrium. Given the volumes of culture media in the insert (total 0.5 mL) and the well (1 mL), C_∞ equals $C_0/3$, where C_0 is the initial concentration of the macromolecule loaded onto the insert.

The macromolecules used in this study are as follows: FITC-dextrans with an average molecular weight of 70 kDa, 150 kDa, or 2000 kDa, FITC-labeled bovine albumin, and FITC-labeled human IgG (all from Sigma–Aldrich; 4 mg mL^{-1} in PBS). The hydrodynamic radii of FITC-dextran (70 kDa, 150 kDa, or 2000 kDa), FITC-albumin, and FITC-IgG are reported to be ∼6, ∼8, ∼27, ∼3, and ∼5 nm, respectively [42, 43].

Whether WZ4003 synergized with fasudil in improving macromolecular permeability was assessed by treating 3D-PDAC fibrotic tissues with a combination of the two inhibitors each at a concentration of 0, 1, 3, or 10 μM, resulting in a 4 × 4 concentration matrix. Synergy scores were calculated using SynergyFinder Plus [31].

4.9 | Assessment of the Macromolecular Drug Delivery Through 3D-PDAC Fibrotic Tissues

Macromolecular drug delivery through 3D-PDAC fibrotic tissues was assessed as previously described [15]. Briefly, WZ4003 was administered on day 1 and day 2 post 3D-PDAC fibrotic tissue generation. After pretreatment for 48 h, culture media containing WZ4003 were replaced as follows: 0.5 mL media with either Doxil or Abraxane inside the insert and 1 mL media within the well. Of note, Doxil and Abraxane were both used at 10 μg mL^{-1}, which is below the reported C_{max} values in patients [44, 45] and does not affect fibrotic tissue thickness [15]. The 3D-PDAC fibrotic tissues were incubated for another 24 h, after which the inserts were

carefully removed and discarded. Media within the wells were collected and used to treat MiaPaCa-2 cells seeded onto 6-well plates (1×10^5/well) or 24-well plates (2×10^4/well) for 48 h. Untreated MiaPaCa-2 cells as well as MiaPaCa-2 cells directly treated with Doxil or Abraxane at C_∞ (i.e., 3.3 μg mL^{-1}) were included as negative and positive controls. MiaPaCa-2 cells were then fixed and stained with crystal violet as described above.

4.10 | Reverse Transcription-Quantitative Polymerase Chain Reaction (RT-qPCR)

PSCs (1×10^5/well) were seeded onto 6-well plates. PSCs were transfected with siRNAs 24 h after cell seeding, as described above. FastGene RNA Basic Kit (Nippon Genetics Co., Ltd., Tokyo, Japan) was used to isolate total RNA 48 h after siRNA transfection. ReverTra Ace -α- (TOYOBO, Osaka, Japan) was used to reverse transcribe total RNA (1 μg) to complementary DNA, according to the manufacturer's protocol. THUNDERBIRD SYBR qPCR mix (TOYOBO) was used for RT-qPCR on the StepOne Plus real-time PCR system (Applied Biosystems, Foster City, CA, USA). Primer sequences are as follows (all primers obtained from Sigma Genosys): *ACTA2* (Forward: 5′-CACCATCGGAAATGAACGTTT-3′; Reverse: 5′-GACTCCATCCCGATGAAGGA-′), *ACTB* (Forward: 5′-TCACCCACACTGTGCCCATCTACGA-3′; Reverse: 5′-CAGCGGAACCGCTCATTGCCAATGG-3′), *CTGF* (Forward: 5′-ATTAGAGCCAACTGCCTGGTC-3′; Reverse: 5′-TGCAGCCAGAAAGCTCAAAC-3′), *COL1A1* (Forward: 5′-CCCTGGAAAGAATGGAGATG-3′; Reverse: 5′-CCATCCAAACCACTGAAACC-3′), *COL1A2* (Forward: 5′-TGCTGGCAAACATGGAAACC-3′; Reverse: 5′-TTATCGCCACGAATGCCTTG-3′), NUAK1 (Forward: 5′-TTGCTGACTTTGGGCTTTCC-3′; Reverse: 5′-TGCTGATTTGCCGAATGAGG-3′), NUAK2 (Forward: 5′-TGGTGGCCATCAAGTCAATC-3′; Reverse: 5′-TCACGATCTTGCTGCTGTTC-3′), *ROCK2* (Forward: 5′-TGACCTCAAACAGTCACAGC-3′; Reverse: 5′-TTTGTGTAAGGCAGCGCTTC-3′), *SMAD2* (Forward: 5′-AACCTTCCATGCATCACAGC-3′; Reverse: 5′-AATTGGGGCTCTGCACAAAG-3′), *SMAD3* (Forward: 5′-TTCAACAACCAGGAGTTCGC-3′; Reverse: 5′-TTGTCAAGCCACTGCAAAGG-3′), and *YAP1* (Forward: 5′-AAGCATGAGCAGCTACAGTG-3′; Reverse: 5′-ACATTTGTCCCAGGAATGGC-3′). For all RT-qPCR experiments, *ACTB* was used as the internal control to normalize gene expression across experimental conditions.

4.11 | Statistical Analysis

GraphPad Prism 10 (GraphPad Software, Inc., La Jolla, CA, USA) was used for all statistical analyses. All statistical tests were two-tailed, and details are provided in the respective figure legend. Statistical significance was set at $p < 0.05$ for all analyses. All samples were included for analyses, and sample sizes are shown as individual data points in the figure or otherwise detailed in the figure legends. Graphs presenting quantified fluorescence intensities are presented as SuperPlots [22], color-coded to represent the intercellular variation observed in each experimental replicate. All quantitative data are shown as mean ± standard deviation (SD).

Author Contributions

Misaki Nakamura: conceptualization, formal analysis, investigation, methodology, writing – review and editing. **Hiroyoshi Y. Tanaka:** conceptualization, data curation, formal analysis, funding acquisition, investigation, methodology, project administration, resources, software, validation, visualization, writing – original draft, writing – review and editing. **Mayu Ohira:** formal analysis, investigation, writing – review and editing. **Haruko Ohta-Okano:** methodology, software, writing – review and editing. **Reika Nakamura:** investigation, writing – review and editing. **Yu Seno:** investigation, writing – review and editing. **Saaya Yara:** investigation, writing – review and editing. **Sakura Fujita:** investigation, writing – review and editing. **Daichi Shibata**: investigation, writing – review and editing. **Masaya Yamamoto:** funding acquisition, writing – review and editing. **Shinichi Toyooka:** resources, writing – review and editing. **Kensuke Osada:** funding acquisition, writing – review and editing. **Horacio Cabral**: conceptualization, writing – review and editing. **Atsushi Masamune:** funding acquisition, resources, writing – review and editing. **Mitsunobu R. Kano:** funding acquisition, resources, supervision, writing – review and editing.

Acknowledgments

This study was supported in part by Grants-in-Aid for Scientific Research (KAKENHI) from the Japan Society for the Promotion of Science (HYT: JP23K06279 and JP20K16989, MY: JP24H00787, KO: JP17KK0102, JP21H03832, JP21K19014, and JP24K03290, MRK: JP23H02653 and JP26293119), Okayama University (HYT and MRK), MEXT Quantum Leap Flagship Program (MEXT Q-LEAP; KO: JPMXS0120330644), Japan Science and Technology Agency (JST) through the open innovation platform for industry-academia co-creation program (COI-NEXT; KO: JPMJPF2202), the Japan Agency for Medical Research and Development (AMED; KO: JP25ym0126804), the Harmonic Ito Foundation (HYT), the Inamori Foundation (HYT), the Research Foundation for Pharmaceutical Sciences (HYT), and the Ryobi Teien Memory Foundation (HYT and MRK). The authors deeply thank Dr. Hiromi Matsubara (National Hospital Organization Okayama Medical Center) for the generous provision of experimental facilities. Further thanks to past and present members of the lab, especially Maho Hashida and Moe Kitamura.

Funding

This work was supported by Japan Society for the Promotion of Science (JP23K06279, JP20K16989, JP24H00787, JP17KK0102, JP21H03832, JP21K19014, JP24K03290, JP23H02653, JP26293119), Ministry of Education, Culture, Sports, Science and Technology (JPMXS0120330644), Japan Science and Technology Agency (JPMJPF2202), Japan Agency for Medical Research and Development (JP25ym0126804), Harmonic Ito Foundation, Inamori Foundation, Research Foundation for Pharmaceutical Sciences, and Ryobi Teien Memory Foundation.

Conflicts of Interest

The authors declare no conflicts of interest.

Data Availability Statement

The data that support the findings of this study are available from the corresponding author upon reasonable request.

References

1. A. J. Grossberg, L. C. Chu, C. R. Deig, et al., "Multidisciplinary Standards of Care and Recent Progress in Pancreatic Ductal Adenocarcinoma," *CA: A Cancer Journal for Clinicians* 70 (2020): 375–403, https://doi.org/10.3322/caac.21626.

2. H. Y. Tanaka, T. Nakazawa, A. Enomoto, A. Masamune, and M. R. Kano, "Therapeutic Strategies to Overcome Fibrotic Barriers to Nanomedicine in the Pancreatic Tumor Microenvironment," *Cancers* 15 (2023): 724, https://doi.org/10.3390/cancers15030724.

3. R. Ando, A. Sakai, T. Iida, K. Kataoka, Y. Mizutani, and A. Enomoto, "Good and Bad Stroma in Pancreatic Cancer: Relevance of Functional States of Cancer-Associated Fibroblasts," *Cancers* 14 (2022): 3315, https://doi.org/10.3390/cancers14143315.

4. M. Erkan, G. Adler, M. V. Apte, et al., "StellaTUM: Current Consensus and Discussion on Pancreatic Stellate Cell Research," *Gut* 61 (2012): 172–178, https://doi.org/10.1136/gutjnl-2011-301220.

5. M. B. Omary, A. Lugea, A. W. Lowe, and S. J. Pandol, "The Pancreatic Stellate Cell: A Star on the Rise in Pancreatic Diseases," *The Journal of Clinical Investigation* 117 (2007): 50–59, https://doi.org/10.1172/JCI30082.

6. G. L. Skalka, D. Whyte, D. Lubawska, and D. J. Murphy, "NUAK: Never Underestimate a Kinase," *Essays in Biochemistry* 68 (2024): 295–307, https://doi.org/10.1042/EBC20240005.

7. M. Faisal, J. H. Kim, K. H. Yoo, E. J. Roh, S. S. Hong, and S. H. Lee, "Development and Therapeutic Potential of NUAKs Inhibitors," *Journal of Medicinal Chemistry* 64 (2021): 2–25, https://doi.org/10.1021/acs.jmedchem.0c00533.

8. T. Zhang, X. He, L. Caldwell, et al., "NUAK1 Promotes Organ Fibrosis via YAP and TGF-β/SMAD Signaling," *Science Translational Medicine* 14 (2022): eaaz4028, https://doi.org/10.1126/scitranslmed.aaz4028.

9. H. Y. Tanaka, T. Nakazawa, T. Miyazaki, H. Cabral, A. Masamune, and M. R. Kano, "Targeting ROCK2 Improves Macromolecular Permeability in a 3D Fibrotic Pancreatic Cancer Microenvironment Model," *Journal of Controlled Release* 369 (2024): 283–295, https://doi.org/10.1016/j.jconrel.2024.03.041.

10. H. Y. Tanaka, T. Kurihara, T. Nakazawa, M. Matsusaki, A. Masamune, and M. R. Kano, "Heterotypic 3D Pancreatic Cancer Model with Tunable Proportion of Fibrotic Elements," *Biomaterials* 251 (2020): 120077.

11. C. Kolliopoulos, E. Raja, M. Razmara, et al., "Transforming Growth Factor β (TGFβ) Induces NUAK Kinase Expression to Fine-Tune Its Signaling Output," *The Journal of Biological Chemistry* 294 (2019): 4119–4136, https://doi.org/10.1074/jbc.RA118.004984.

12. W.-C. Yuan, B. Pepe-Mooney, G. G. Galli, et al., "NUAK2 Is a Critical YAP Target in Liver Cancer," *Nature Communications* 9 (2018): 4834, https://doi.org/10.1038/s41467-018-07394-5.

13. H. Y. Tanaka, K. Kitahara, N. Sasaki, et al., "Pancreatic Stellate Cells Derived from Human Pancreatic Cancer Demonstrate Aberrant SPARC-Dependent ECM Remodeling in 3D Engineered Fibrotic Tissue of Clinically Relevant Thickness," *Biomaterials* 192 (2019): 355–367, https://doi.org/10.1016/j.biomaterials.2018.11.023.

14. K. P. Olive, M. A. Jacobetz, C. J. Davidson, et al., "Inhibition of Hedgehog Signaling Enhances Delivery of Chemotherapy in a Mouse Model of Pancreatic Cancer," *Science* 324 (2009): 1457–1461, https://doi.org/10.1126/science.1171362.

15. M. Ohira, M. Kitamura, H. Iwasaki, et al., "Collagen Signaling via DDR1 Exacerbates Barriers to Macromolecular Drug Delivery in a 3D Model of Pancreatic Cancer Fibrosis," *Small* 21 (2025): e06926, https://doi.org/10.1002/smll.202506926.

16. S. Banerjee, S. J. Buhrlage, H.-T. Huang, et al., "Characterization of WZ4003 and HTH-01-015 as Selective Inhibitors of the LKB1-Tumour-Suppressor-Activated NUAK Kinases," *Biochemical Journal* 457 (2014): 215–225, https://doi.org/10.1042/BJ20131152.

17. C. Jensen and Y. Teng, "Is It Time to Start Transitioning From 2D to 3D Cell Culture?," *Frontiers in Molecular Biosciences* 7 (2020): 33, https://doi.org/10.3389/fmolb.2020.00033.

18. G. Murphy, D. J. Brayden, D. L. Cheung, A. Liew, M. Fitzgerald, and A. Pandit, "Albumin-Based Delivery Systems: Recent Advances, Challenges, and Opportunities," *Journal of Controlled Release* 380 (2025): 375–395, https://doi.org/10.1016/j.jconrel.2025.01.035.

19. C. M. Dawidczyk, C. Kim, J. H. Park, et al., "State-of-the-Art in Design Rules for Drug Delivery Platforms: Lessons Learned from FDA-Approved Nanomedicines," *Journal of Controlled Release* 187 (2014): 133–144, https://doi.org/10.1016/j.jconrel.2014.05.036.

20. N. V. Rajeshkumar, S. Yabuuchi, S. G. Pai, et al., "Superior Therapeutic Efficacy of Nab-Paclitaxel over Cremophor-Based Paclitaxel in Locally Advanced and Metastatic Models of Human Pancreatic Cancer," *British Journal of Cancer* 115 (2016): 442–453, https://doi.org/10.1038/bjc.2016.215.

21. D. R. Stirling, M. J. Swain-Bowden, A. M. Lucas, A. E. Carpenter, B. A. Cimini, and A. Goodman, "CellProfiler 4: Improvements in Speed, Utility and usability," *BMC Bioinformatics* 22 (2021): 433, https://doi.org/10.1186/s12859-021-04344-9.

22. S. J. Lord, K. B. Velle, R. D. Mullins, and L. K. Fritz-Laylin, "SuperPlots: Communicating Reproducibility and Variability in Cell Biology," *The Journal of Cell Biology* 219 (2020): e202001064, https://doi.org/10.1083/jcb.202001064.

23. S. Ricard-Blum, "The Collagen Family," *Cold Spring Harbor Perspectives in Biology* 3 (2011): a004978, https://doi.org/10.1101/cshperspect.a004978.

24. M. K. Gill, T. Christova, Y. Y. Zhang, et al., "A Feed Forward Loop Enforces YAP/TAZ Signaling during Tumorigenesis," *Nature Communications* 9 (2018): 3510, https://doi.org/10.1038/s41467-018-05939-2.

25. B. Zhao, X. Ye, J. Yu, et al., "TEAD Mediates YAP-Dependent Gene Induction and Growth Control," *Genes & Development* 22 (2008): 1962–1971, https://doi.org/10.1101/gad.1664408.

26. H. Hayashi, S. Abdollah, Y. Qiu, et al., "The MAD-Related Protein Smad7 Associates with the TGFbeta Receptor and Functions as an Antagonist of TGFbeta Signaling," *Cell* 89 (1997): 1165–1173, https://doi.org/10.1016/s0092-8674(00)80303-7.

27. A. Nakao, M. Afrakhte, A. Morén, et al., "Identification of Smad7, a TGFbeta-Inducible Antagonist of TGF-Beta Signalling," *Nature* 389 (1997): 631–635, https://doi.org/10.1038/39369.

28. T. Vallenius, K. Vaahtomeri, B. Kovac, A.-M. Osiceanu, M. Viljanen, and T. P. Mäkelä, "An Association between NUAK2 and MRIP Reveals a Novel Mechanism for Regulation of Actin Stress Fibers," *Journal of Cell Science* 124 (2011): 384–393, https://doi.org/10.1242/jcs.072660.

29. Z. Qin, G. J. Fisher, J. J. Voorhees, and T. Quan, "Actin Cytoskeleton Assembly Regulates Collagen Production via TGF-β Type II Receptor in Human Skin Fibroblasts," *Journal of Cellular and Molecular Medicine* 22 (2018): 4085–4096, https://doi.org/10.1111/jcmm.13685.

30. S. Tojkander, G. Gateva, and P. Lappalainen, "Actin Stress Fibers – Assembly, Dynamics and Biological Roles," *Journal of Cell Science* 125 (2012): 1855–1864, https://doi.org/10.1242/jcs.098087.

31. S. Zheng, W. Wang, J. Aldahdooh, et al., "SynergyFinder Plus: Toward Better Interpretation and Annotation of Drug Combination Screening Datasets," *Genomics, Proteomics & Bioinformatics* 20 (2022): 587–596, https://doi.org/10.1016/j.gpb.2022.01.004.

32. X. Wang, Z. Song, F. Chen, et al., "AMPK-Related Kinase 5 (ARK5) Enhances Gemcitabine Resistance in Pancreatic Carcinoma by Inducing Epithelial-Mesenchymal Transition," *American Journal of Translational Research* 10 (2018): 4095–4106.

33. R. Wang, D. Su, Y. Liu, et al., "The NF-κB/NUAK2 Signaling Axis Regulates Pancreatic Cancer Progression by Targeting SMAD2/3," *iScience* 27 (2024): 109406, https://doi.org/10.1016/j.isci.2024.109406.

34. M.-S. Seo, K. H. Jung, K. Kim, et al., "Discovery of a Novel NUAK1 Inhibitor against Pancreatic Cancer," *Biomedicine & Pharmacotherapy* 152 (2022): 113241, https://doi.org/10.1016/j.biopha.2022.113241.

35. D. Whyte, G. Skalka, P. Walsh, et al., "NUAK1 Governs Centrosome Replication in Pancreatic Cancer via MYPT1/PP1β and GSK3β-Dependent Regulation of PLK4," *Molecular Oncology* 17 (2023): 1212–1227, https://doi.org/10.1002/1878-0261.13425.

36. R. A. J. van de Vis, A. Moustakas, and L. P. van der Heide, "NUAK1 and NUAK2 Fine-Tune TGF-β Signaling," *Cancers* 13 (2021): 3377, https://doi.org/10.3390/cancers13133377.

37. B. Hinz, G. Celetta, J. J. Tomasek, G. Gabbiani, and C. Chaponnier, "Alpha-Smooth Muscle Actin Expression Upregulates Fibroblast Contractile Activity," *Molecular Biology of the Cell* 12 (2001): 2730–2741.

38. S. Sakai, C. Iwata, H. Y. Tanaka, et al., "Increased Fibrosis and Impaired Intratumoral Accumulation of Macromolecules in a Murine Model of Pancreatic Cancer Co-Administered with FGF-2," *Journal of Controlled Release* 230 (2016): 109–115, https://doi.org/10.1016/j.jconrel.2016.04.007.

39. H. Y. Tanaka and M. R. Kano, "Stromal Barriers to Nanomedicine Penetration in the Pancreatic Tumor Microenvironment," *Cancer Science* 109 (2018): 2085–2092, https://doi.org/10.1111/cas.13630.

40. S. Hamada, A. Masamune, T. Takikawa, et al., "Pancreatic Stellate Cells Enhance Stem Cell-Like Phenotypes in Pancreatic Cancer Cells," *Biochemical and Biophysical Research Communications* 421 (2012): 349–354, https://doi.org/10.1016/j.bbrc.2012.04.014.

41. J. Kolega, "Phototoxicity and Photoinactivation of Blebbistatin in UV and Visible Light," *Biochemical and Biophysical Research Communications* 320 (2004): 1020–1025, https://doi.org/10.1016/j.bbrc.2004.06.045.

42. J. Ambati, C. S. Canakis, J. W. Miller, et al., "Diffusion of High Molecular Weight Compounds through Sclera," *Investigative Ophthalmology & Visual Science* 41 (2000): 1181–1185.

43. L. Lebrun and G.-A. Junter, "Diffusion of Dextran through Microporous Membrane Filters," *Journal of Membrane Science* 88 (1994): 253–261, https://doi.org/10.1016/0376-7388(94)87011-X.

44. O. Lyass, A. Hubert, and A. A. Gabizon, "Phase I Study of Doxil-Cisplatin Combination Chemotherapy in Patients with Advanced malignancies," *Clinical Cancer Research* 7 (2001): 3040–3046.

45. E. R. Gardner, W. L. Dahut, C. D. Scripture, et al., "Randomized Crossover Pharmacokinetic Study of Solvent-Based Paclitaxel and Nab-Paclitaxel," *Clinical Cancer Research* 14 (2008): 4200–4205, https://doi.org/10.1158/1078-0432.CCR-07-4592.

Supporting Information

Additional supporting information can be found online in the Supporting Information section. **Supporting Fig. S1: Pharmacological inhibition of NUAK1/2 kinases in primary PSCs enhances macromolecular permeability of 3D-PDAC fibrotic tissues through regulation of collagen I expression.** (**A-D**) Effect of WZ4003 on the proliferation of primary PSCs (prPSCs). (**E-H**) Representative 3D-reconstructed images (**E,F**) and measured thickness (**G,H**) of WZ4003-treated 3D-PDAC fibrotic tissues. $n = 8$ thickness measurements. Scale bars = 100 μm (horizontal) and 20 μm (vertical). (**I,J**) Permeability of WZ4003-treated 3D-PDAC fibrotic tissues to 2000 kDa FITC-dextran. (**K**) Immunofluorescent staining for αSMA (red) in WZ4003-treated prPSCs. Nuclei (blue) were stained with Hoechst 33342. (**L,M**) Mean αSMA fluorescence per cell in WZ4003-treated prPSCs. (**N**) WZ4003-treated pr PSCs were immunofluorescently stained for collagen I (green) and β-tubulin (red). Nuclei (blue) were stained with Hoechst 33342. (**O,P**) Mean collagen I fluorescence per cell in WZ4003-treated prPSCs. In (**K**) and (**N**), scale bars = 100 μm. One-way ANOVA with *post hoc* Dunnett's multiple comparisons test was performed with 0 μM as the reference condition, and *n.s.*, *, **, ***, and **** denote not significant, $p < 0.05$, $p < 0.01$, $p < 0.001$, and $p < 0.0001$, respectively. **Supporting Fig. S2: Diminution of collagen I in PSCs upon NUAK1/2 inhibition is upstream of diminished αSMA expression.** (**A-F**) Reverse-transcription polymerase chain reaction (RT-qPCR) analysis of *ACTA2* (**A,B**), *COL1A1* (**C,D**), and *COL1A2* (**E,F**) mRNA expressions in WZ4003-treated PSCs. (**G,H**) *ACTA2* mRNA expression in PSCs treated with siCOL1A1, siCOL1A2, or siCOL1A1+2. (**I-L**) *COL1A1* (**I,J**) and *COL1A2* (**K,L**) mRNA expression in PSCs treated with siACTA2. (**M**) Immunofluorescent staining for αSMA (red) in PSCs treated with siACTA2 or siCOL1A1+2. Nuclei (blue) were stained with Hoechst 33342. (**N,O**) Mean αSMA fluorescence per cell in PSCs treated as in (**M**). (**P**) Immunofluorescent staining for collagen I (green) and β-tubulin (red) in PSCs treated with siACTA2 or siCOL1A1+2. Nuclei (blue) were stained with Hoechst 33342. (**Q,R**) Mean collagen I fluorescence per cell in PSCs treated as in (**J**). In all RT-qPCR data, $n = 3$ biological replicates. Scale bars = 100 μm. In (**I**)-(**L**), Student's un-paired *t*-test with Welch's correction was performed. In all other graphs, one-way ANOVA with *post hoc* Dunnett's multiple comparisons test was performed with 0 μM or ctrl siRNA as the reference condition. In all graphs, *n.s.*, *, **, ***, and **** denote not significant, $p < 0.05$, $p < 0.01$, $p < 0.001$, and $p < 0.0001$, respectively. **Supporting Fig. S3: RT-qPCR analysis of knockdown efficiencies of the siRNAs used in this study.** (**A,B**) *ACTA2* mRNA expression in PSCs treated with siACTA2. (**C-F**) *COL1A1* (**C, D**) and *COL1A2* (**E,F**) mRNA expressions in PSCs treated with siCOL1A1, siCOL1A2, or siCOL1A1+2. (**G,H**) NUAK1 mRNA expression in PSCs treated with siNUAK1 or siNUAK2. (**I,J**) NUAK2 mRNA expression in PSCs treated with siNUAK1, siNUAK2, siROCK2, or siNUAK2+ROCK2. (**K,L**) *YAP1* mRNA expression in PSCs treated with siYAP1. (**M-P**) *SMAD2* (**M,N**) and *SMAD3* (**O,P**) mRNA expressions in PSCs treated with siSMAD2, siSMAD3, or a 1:1 mixture of siSMAD2 and siSMAD3 (siSMAD2+3). (**Q,R**) *ROCK2* mRNA expression in PSCs treated with siNUAK2, siROCK2, or siNUAK2+ROCK2. Student's un-paired *t*-test with Welch's correction was performed in (**A**), (**B**), (**K**), and (**L**). In all other graphs, one-way ANOVA with *post hoc* Dunnett's multiple comparisons test was performed with ctrl siRNA as the reference condition. In all graphs, *n.s.*, *, **, ***, and **** denote not significant, $p < 0.05$, $p < 0.01$, $p < 0.001$, and $p < 0.0001$, respectively. **Supporting Fig. S4: NUAK2 knockdown diminishes collagen I expression in prPSCs.** (**A**) Immunofluorescent staining for collagen I (green) and β-tubulin (red) in prPSCs treated with siNUAK1 or siNUAK2. Nuclei (blue) were stained with Hoechst 33342. Scale bars = 100 μm. (**B,C**) Mean collagen I fluorescence per cell in prPSCs treated as in (**A**). One-way ANOVA with *post hoc* Dunnett's multiple comparisons test was performed with ctrl siRNA as the reference condition, and *n.s.*, **, and *** denote not significant, $p < 0.01$, and $p < 0.001$, respectively. **Supporting Fig. S5: Effect of *YAP1* or *SMAD2/3* knockdown on collagen I expression in PSCs.** (**A-D**) Effect of siYAP1 (**A,B**), siSMAD2, siSMAD3, or siSMAD2+3 (**C, D**) on PSC growth. (**E-H**) Effect of siYAP1 (**E,F**), siSMAD2, siSMAD3, or siSMAD2+3 (**G,H**) on 3D-PDAC fibrotic tissue thickness. (**I-L**) Permeability to 2000 kDa FITC-dextran of 3D-PDAC fibrotic tissues constructed from PSCs treated with siYAP1 (**I,J**), siSMAD2, siSMAD3, or siSMAD2+3 (**K,L**). (**M,N**) Immunofluorescent staining for collagen I (green) and β-tubulin (red) in PSCs treated with siYAP1. Nuclei (blue) were stained with Hoechst 33342. (**O,P**) Mean collagen I fluorescence per cell in PSCs treated as in (**M,N**). (**Q,R**) Immunofluorescent staining for collagen I (green) and β-tubulin (red) in PSCs treated with siSMAD2, siSMAD3, or siSMAD2+3. Nuclei (blue) were stained with Hoechst 33342. (**S,T**) Mean collagen I fluorescence per cell in PSCs treated as in (**Q,R**). Scale bars = 100 μm. Student's un-paired *t*-test with Welch's correction was performed in experiments involving siYAP. In all other graphs, one-way ANOVA with *post hoc* Dunnett's multiple comparisons test was performed with ctrl siRNA as the reference condition. In all graphs, *n.s.*, *, **, ***, and **** denote not significant, $p < 0.05$, $p < 0.01$, $p < 0.001$, and $p < 0.0001$, respectively. **Supporting Fig. S6: Targeting of NUAK2 in prPSCs diminishes stress fibers**. (**A**) Staining of filamentous actin with phalloidin (green) in WZ4003-treated prPSCs. Nuclei (blue) were stained with Hoechst 33342. (**B,C**) Mean phalloidin fluorescence per cell in WZ4003-treated prPSCs. (**D**) Phalloidin (green) and Hoechst 33342 (blue) staining of prPSCs treated with ctrl siRNA, siNUAK1, or siNUAK2. (**E,F**) Mean phalloidin fluorescence per cell in prPSCs treated with siNUAK1 or siNUAK2. Scale bars = 100 μm. One-way ANOVA with *post hoc* Dunnett's multiple comparisons test was performed with 0 μM or ctrl siRNA as the reference condition, and *n.s.*, *, **, and *** denote not significant, $p < 0.05$, $p < 0.01$, and $p < 0.001$, respectively. **Supporting Fig. S7: Induction of stress fiber disassembly by ML-7 diminishes collagen I expression by PSCs to enhance macromolecular permeability of 3D-PDAC fibrotic**

tissues. (**A**) PSCs treated with the myosin light chain kinase inhibitor ML-7 were stained with phalloidin (green) and Hoechst 33342 (nuclei; blue). (**B,C**) Mean phalloidin fluorescence per cell in ML-7-treated PSCs. (**D**) Immunofluorescent staining for collagen I (green) and β-tubulin (red) in ML-7-treated PSCs. Nuclei (blue) were stained with Hoechst 33342. (**E,F**) Mean collagen I fluorescence per cell in ML-7-treated PSCs. (**G,H**) Effect of ML-7 on PSC growth. (**I-L**) Thickness (**I,J**) and permeability to 2000 kDa FITC-dextran (**K,L**) of ML-7-treated 3D-PDAC fibrotic tissues. $n = 8$ thickness measurements. Scale bars = 100 μm. One-way ANOVA with *post hoc* Dunnett's multiple comparisons test was performed with 0 μM as the reference condition, and *n.s.*, *, **, ***, and **** denote not significant, $p < 0.05$, $p < 0.01$, $p < 0.001$, and $p < 0.0001$, respectively. **Supporting Fig. S8: Disturbing actin stress fibers in prPSCs diminishes collagen I expression to enhance macromolecular permeability of 3D-PDAC fibrotic tissues.** (**A**) Phalloidin (green) and Hoechst 33342 (blue) staining of prPSCs treated with 10 μM blebbistatin, 10 μM ML-7, or vehicle control (DMSO). (**B,C**) Mean phalloidin fluorescence per cell in prPSCs treated as in (**A**). (**D**) Immunofluorescent staining of collagen I (green) and β-tubulin (red) in prPSCs treated with 10 μM blebbistatin or 10 μM ML-7. Nuclei (blue) were stained with Hoechst 33342. (**E,F**) Mean collagen I fluorescence per cell in prPSCs treated as in (**D**). (**G,H**) Effect of blebbistatin on the proliferation of prPSCs. (**I,J**) Effect of ML-7 on the proliferation of prPSCs. (**K-N**) Thickness (**K,L**) and permeability to 2000 kDa FITC-dextran (**M, N**) of 3D-PDAC fibrotic tissues treated with 10 μM blebbistatin, 10 μM ML-7, or DMSO. $n = 8$ thickness measurements. Scale bars = 100 μm. One-way ANOVA with *post hoc* Dunnett's multiple comparisons test was performed with DMSO as the reference condition, and *n.s.*, *, **, ***, and **** denote not significant, $p < 0.05$, $p < 0.01$, $p < 0.001$, and $p < 0.0001$, respectively.